ECOLE POLYTECHNIQUE FEDERALE DE LAUSANNE
SCHOOL OF LIFE SCIENCES

Master in Bioengineering and Biotechnology

Vertically aligned carbon nanotubes for supercapacitor and the effect of surface functionalization to its performance

Carried out in the Charyk laboratory for Bio-inspired designs
At California Institute of Technology

Under the supervision of Pr Morteza Gharib

Done by

MELANIE ELISA GUITTET

Under the direction of:
Pr Jürgen Brugger
In the laboratory of Microsystems

External expert: Pr Morteza Gharib, California Institute of Technology

Abstract

Keywords: electrochemical capacitors, energy storage, vertically-aligned carbon nanotubes, functionalization, long lifetime

As reliable mobile energy sources became more and more needed and alternative energy demands became more prevalent, the research in advanced energy storage technologies turned into a topic of utmost importance in today's society. Innovative electrode materials that are able to provide increased energy densities and long lifetime must be then be developed. Nanomaterials such as carbon nanotubes are of tremendous prospects in that context. This master thesis aims at realizing an electrochemical capacitor using a vertically grown carbon nanotube array, which is used as electrode in different sets of experiments to evaluate its electrical energy storage capability. Cyclic voltammetry and electrochemical impedance spectroscopy are used to determine the specific capacitance of the device, which is composed of two nanotubes electrodes separated by a polypropylene filter, in an adequate electrolyte. The surface chemistry was modified by adding hydroxyl groups onto the nanotubes surface, thus making them hydrophilic and providing an efficient way to increase their storage ability by a factor of two to three. Different electrolytes were compared, both aqueous and non aqueous, and the important parameter in choosing an appropriate electrolyte for a high storage ability was shown to be the polarity of the solution. The carried out performance studies gave encouraging results with a maximum energy density of 21 Wh/kg at a power density of 1.1 kW/kg for a hydrophilic electrode using tetraethylammonium tetrafluoroborate in propylene carbonate. Respectively, a maximum power density was found to be 22 kW/kg at energy density of $\sim$2 Wh/kg for a hydrophobic sample.

This device can be claimed to be entirely carbon-based, with a relatively small ecological print compared to most lithium-based capacitors and inexpensive. The lifetime is also extremely long, indeed more than hundreds of thousands cycles without failure have been achieved.

Acknowledgements

I would like to thank everyone who helped me achieving this project, as well as supported me during my entire academic curriculum, both in EPFL and in Caltech.

My first thanks will go to my supervisors, first Pr Jürgen Brugger, who was able to help me in any kind of situations, and to follow my progress with both time and consideration when I needed support. I am extremely grateful for the cordial supervision as well as his a high availability and judicious advices. I would also like to thank Pr Morteza Gharib, to have offered me a very pleasant working environment, and to have let me discover new fields where my knowledge had to be constantly challenged and renewed.

I would like to warmly thank Indrat for the supervision and help he was able to offer during this entire project, for his numerous advices and his endless availability, even at 3:00am before the submission for IEEE.

My thanks also go towards the entire team of the Charyk Lab, who offered a very dynamic and productive frame to my research, as well as numerous helping hands in addition to nice discussions in the clean room.

I would like to thank also my friends at Caltech, with whom I feel like I shared one of the best year of my life, and my parents, who supported me and believed in me during my entire studies. And finally, Oli, thank you for your eternal approval and support, without which this project could not have been brought to fruition.

Contents

List of Figures

LIST OF FIGURES

List of Tables

Glossary

AC Alternating current. 17

Ag Silver. 29, 30

Al_2O_3 Aluminium oxide. 41

CE Counter electrode. 16

CNT Carbon nanotubes. 3, 12–14, 36–38, 43, 50, 56

CO_2 Carbon dioxide. 1

COOH Carboxylic group used to functionalize the carbon nanotubes. 13

CV Cyclic voltammetry. 19, 22, 24

CVD Chemical vapor deposition. 11

EC Ethylene carbonate. 25

EDLC Electrical double-layer capacitance. 5, 6, 8, 17, 56

EDS Energy-dispersive X-ray spectroscopy. 50, 51

EIS Electrochemical Impedance Spectroscopy. 17–20, 36

Et_4NBF_4 Tetraethylammonium tetrafluoroborate. 25, 27, 30, 32, 33, 35–38, 42, 46

Fe Iron. 41

H_2SO_4 Sulfuric acid. 36

$HiCNT_f$ Hydrophilic nanotubes functionalized with fullerenes. 53

$HoCNT_f$ Hydrophobic nanotubes functionalized with fullerenes. 53

KOH Potassium hydroxide. 23, 24, 36–38, 46

$LiBF_4$ Lithium tetrafluoroborate. 38

$LiPF_6$ Lithium Hexafluorophosphate. 45

MnO_2 Manganese dioxide. 53

OH Hydroxyl group used to functionalize the nanotubes. 13, 37, 52, 53

PC Propylene carbonate. 25, 27, 30, 32, 33, 35–38, 43

Pd Palladium. 21, 29, 30

PDMS Polydimethylsiloxane, a polymeric silicon. 12, 13, 21

Pt Platinum. 16, 21, 29, 30

PTFE Polytetrafluoroethylene. 40

SEM Scanning electron microscope. 21, 28, 29, 31, 50, 51

SnO_2 Tin dioxide. 50

TEM Transmission electron microscope. 50, 51

TiO_2 Titanium dioxide. 49

UV Ultra violet. 12–14

VANT Vertically-aligned carbon nanotubes. 6, 13, 16, 21, 26, 28–32, 35–39, 43, 44, 51

WE Working electrode. 16

Chapter 1

Introduction

This chapter aims at introducing the context, the problematic and the objectives of this master thesis. It also explores the adopted methodology.

1.1 Energy storage and the challenges of global energy supply

The world energy supply is facing multiple issues, which from individual concerns had become an affair of state. The fast and nearly uncontrollable development of emerging countries, both in terms of improved living standards and economy, has led to a formidable increase in energy needs, and the energy production can hardly follow. Moreover, the unbridled and frantic use of fossil energies is coming to a dead-end: reserves of oil and other non-renewable fuels are starting to be depleted. Consequently, the earth is facing the consequences of this overuse of its resources, and suffering from the climate change due the rising of greenhouse gas emission. Indeed, according to the International Energy Agency statistics, fossil fuels (oil, coal and gas) account for most of the world energy supply, representing 81% (1) of the world energy. This represents 35.2 Gt of CO_2 in 2008 (1). In its reference scenario, the World Energy Outlook projects that world CO_2 emissions from fuel combustion will continue to grow unabated, reaching 40.2 Gt CO_2 by 2030 (2), thus meeting with the worst-case scenario presented by the Intergovernmental Panel on Climate Change (3).

A course of action must be taken to develop new sources of energy, mainly renewable, such as solar energy, wind energy, or even wave energy. Because the sun does not shine during the night, the wind does not blow all the time and at the exact time when we want it, and we want our cars to have at least a couple of hours of autonomy, energy storage systems have become a crucial component in our daily routine. Both these two objectives - development of new green energies and advances in energy storage technologies - are to be met if one can hope facing the environmental issues that our world is now dealing with as well as settle down political tensions over non-renewable fuels.

1.1.1 Scope of study

This project mainly deals with the second objective highlighted in the previous section, aiming at optimizing the efficiency and the reliability of the energy storage.

Supercapacitors (also called electrical double-layer capacitors) offer very promising alternatives compared to batteries and fuel cell to store and deliver energy, mainly because of :

- their extremely long lifetime, that can go up to millions of cycles
- very high rates of charge and discharge : they are fully charged and discharged within seconds
- high power density, around 10 kW/kg

They however suffer from a lower energy density (4), about 5 Wh/kg (5). All these characteristics make them a very valuable asset to meet the increasing demands of energy storage, with uses ranging from consumer electronic devices to hybrid cars. Rather than totally replacing the existing batteries, they will complement them efficiently, since they meet different goals. Supercapacitors utilize the double-layer of charge formed when a voltage is applied to an electrode immersed in a given electrolyte (6). Unlike batteries, which use chemical reactions to store energy, supercapacitors store energy through the physical separation of electrical charges. The electrodes used for supercapacitors are commonly made out of highly porous carbon, like activated carbon. This project chose to use vertically-aligned carbon nanotubes. Carbon nanotubes are of tremendous prospects in a very wide variety of applications, explaining their

broad interest in several fields of research: lightweight spacecraft, drug delivery, molecular sensors, electronic devices, electron field emission, hydrogen storage, nanowires, and supercapacitors are some examples of this huge diversity (7). The main interest in supercapacitors lies in their intrinsically large surface area and their high electrical conductivity. In addition, the cost to produce them is expected to decrease quickly in the future (8). Since only the wetted part of the nanotube can contribute to capacitance, the increase of the effective surface-area in contact with the electrolyte is extremely important. In order to increase the effective surface-area and achieve a maximum performance, the carbon nanotubes have to be modified with appropriate functional groups, which are chosen in accordance to the electrolyte used in the capacitor.

1.1.2 Methodology and outline of the report

The overall goal of this project is to understand the energy storage mechanism involved in a supercapacitor, as well as to improve its performance using the striking properties of vertically aligned carbon nanotubes (CNT).

Chapter 2 consists in the explanation and description of what has been done and achieved in terms of supercapacitor through literature studies, as well as some in-depth characterization of the basic mechanisms involved.

Chapter 3 is dedicated to the understanding of the basic methods used throughout this project, as well as the techniques required.

Chapter 4 explores the characteristics of both the carbon nanotubes and graphite samples used throughout this study, and review comparatively their features, and usefulness when employed as electrodes for supercapacitors.

Results are presented and analyzed in the following chapter (Chapter 5), and some conclusions are shown in details. The last part is devoted to the evaluation of the performance of the device, in terms of power, energy, and lifetime.

Finally, a last chapter (Chapter 6) is dedicated to leads that did not succeed or were not thoroughly looked into, but are worth mentioned and very probable for further investigation had time permitted it.

Chapter 2

Literature review

This chapter goes through the basic knowledge useful for this study. Some theoretical background is underlined, as well as practical comparison with the existing market and technological advances in this field of knowledge.

2.1 Electrochemical double-layer capacitor

Electrochemical capacitors (EDLC, also known as electric double-layer capacitors or supercapacitors) store energy as an electric field of charged particles at the interface between a metal electrode and the electrolyte. Such capacitors can be charged very rapidly and have an extremely long lifetime, which are far more superior to conventional batteries (6). On the contrary, conventional batteries store energy through charge carriers (usually electrons) removed from one metal plate and deposited onto another through a liquid electrolyte, thus creating a potential between the two plates, further harnessed in an external circuit. The liquid viscosity thus hampers the movement of the charge carriers.

Because the storage capacity of a capacitor is proportional to the surface area of the electrodes (9), an enlargement of the effective surface area is necessary to allow the capacitor to store a much larger amount of energy than what is currently achieved by conventional batteries at the same size. The use of carbon nanotubes electrodes is a

very efficient way to answer this issue, since they exhibit a high surface area-to-volume ratio. A sketch of this device is presented on figure 2.1.

2.1.1 Mechanism of action

The most basic model used to describe a supercapacitor is composed of two electrodes immersed in a conductive liquid - or polymer - called the electrolyte. A filter separates the electrodes, acting as an ionic-conducting separator that prevents shorts. (10)

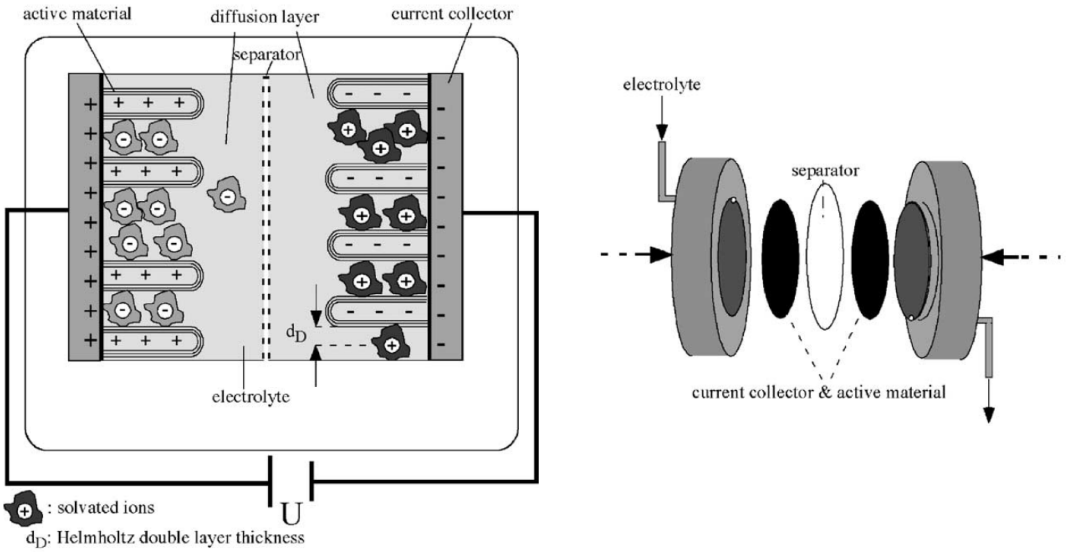

Figure 2.1: Electrochemical double-layer capacitor - (a) Sketch of the electrochemical double-layer capacitor with VANT array electrode (b) Schematic view of the EDLC test cell (11)

Electrochemical double-layer capacitors store the charge electrostatically and releases electric energy through the transfer of ions to and from the electrode/electrolyte interface, usually using materials with a high surface area to maximize and enhance the charge transfer. Charge is described as:

$$Q = CV \tag{2.1}$$

C is the capacitance in Farads [F]
V is voltage applied between the devices terminals in Volts [V]
Q is the capacitor charge in Coulombs [C =A.s=F.V]

Charge separation takes place at the interface between electrode and electrolyte, producing a double-layer capacitance C:

$$C = \frac{\varepsilon_o \varepsilon_r A}{d} \tag{2.2}$$

ε_r electrolyte dielectric constant
ε_o dielectric constant of the vacuum
d effective thickness of the double-layer
A electrode surface area

2.1.2 Useful formulas used

By deriving the first basic formula 2.1, we get:

$$\frac{dQ}{dt} = V\frac{dC}{dt} + C\frac{dV}{dt} \tag{2.3}$$

Assuming the capacitance is constant relatively to time, we obtain:

$$I = C\frac{dV}{dt} \tag{2.4}$$

I current in Amperes [A]
C is the capacitance in Farads [F]
$\frac{dV}{dt}$ the scan rate in mV/s

The energy stored in a capacitor, calculated in Joules [J], is defined as:

$$E = \frac{1}{2}CV^2 \tag{2.5}$$

The power drawn from a capacitor during discharge, in Watts [W], depends on both the capacitor potential and the electrical current:

$$P = UI \Rightarrow P = CV\frac{dV}{dt} \tag{2.6}$$

2.2 Comparison and highlights

Electrochemical double-layer capacitors can deliver a high power output during a extremely long time, despite their comparatively low ability to store energy, which is about 10 to 100 times lower than lead-acid batteries. Carbon represents a very attractive material for use in electrochemical applications, and storage energy in particular: indeed, it boasts a diverse portfolio of useful features, such as:

- Multiple allotropes: graphene, diamond, Buckminsterfullerenes (or buckyballs), nanotubes ...
- Different microstructures, depending on the degree of graphitization.
- Various forms of macrostructures, ranging from powders to foams and composites.
- A high electrical conductivity (except diamond).

Much research is now focusing on supercapacitors since they have both a long cycle life and a high efficiency, as seen on table 2.2. Moreover, the theoretical capacitance is extremely high for supercapacitors with carbon-based electrodes; for instance, the theoretical capacitance that can be achieved with a graphene-based supercapacitor exceeds 550 F/g (12). And finally, the lifetime for supercapacitors is extremely high, up to millions of cycles. This is highlighted on figure 2.2.

Advantages	**Disadvantges**	**Current applications**
Higher charge and discharge rates (high power density)	Higher self-discharge rate	Hybrid Electric Vehicles
Longer cycle life (>100,000 cycles)	Lower energy density	Diesel engine starting systems
Low toxicity materials	Lower cell voltage	Cordless power tools
Operation over a wide temperature range	Poor voltage regulation	Emergency and safety systems
Low cost per cycle	High initial cost	

Table 2.1: Comparison with battery - Overview from GAMRY.

The gravimetric energy density - or in other words the amount of energy that can be stored in a given weight - of commercial supercapacitors is usually around 5-6 Wh/kg, which is about 8 times below the lower limit of batteries (4). However, some recent commercialized supercapacitors are able to withstand up to 30 Wh/kg (Premlis, JEOLs supercapacitor), at the cost of a relatively bulky and heavy device. It is composed of multiple matched series-connected individual EDLC, like series-connected cells in

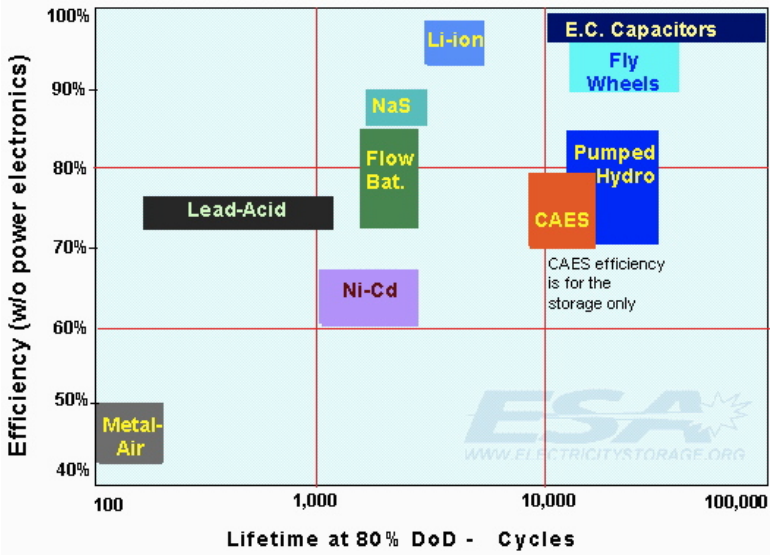

Figure 2.2: Life efficiency - Efficiency and cycle life both affect the overall storage cost. Indeed, low efficiency increases the effective energy cost as only a fraction of the stored energy can be used. Low cycle life also increases the total cost as the device needs to be replaced more often. Taken from the Energy Storage Association.

batteries, rather than one single extremely efficient supercapacitor cell. The use of graphene in a graphene-based supercapacitors allows to go even further beyond these limits, by reaching a specific energy density of ∼85 Wh/kg at room temperature (and 60% more at elevated temperature of 80 °C) (12).

Hence, the performance of supercapacitors rely somewhere in between batteries and traditional capacitors. The advantages and disadvantages of supercapacitors when compared to batteries are summarized in table 2.1.

Table 2.2: Technology comparison and range of application. Taken from the Electricity storage association

Storage technologies	**Main advantages**	**Disadvantages**	**Power application**	**Energy application**
Pumped storage	High capacity, Low cost	Special site requirement		●
Compressed air energy storage	High capacity, Low cost	Special site requirement, Need gas fuel		●
Flow batteries: PSB, VRB, ZnBr	High capacity, Independent Power and Energy ratings	Low energy density	◐	●
Metal-Air	Very high Energy Density	Electric charging is difficult		●
Sodiumsulfur (NaS) battery	High Power and Energy Densities, High Efficiency	Production costs, Safety concerns (addressed in design)	●	●
Li-Ion battery	High Power and Energy Densities, High efficiency	High production costs, Requires special charging circuit	●	○
Nickel-cadmium (Ni-Cd) battery	High Power and Energy Densities, High Efficiency		●	◐
Other advanced batteries	High Power and Energy Densities, High Efficiency	High production costs	●	○
Lead-Acid	Low capital cost	Limited cycle life when deeply discharged	●	○
Flywheels	High power	Low energy density	●	○
Superconducting Magnetic Energy Storage (SMES)	High power	Low energy density, High production costs	●	
Electrochemical Capacitors	Long cycle life, High Efficiency	Low energy density	●	◐

●	◐	○	None
Fully capable and reasonable	Reasonable for this application	Feasible but not quite practical or economical	Not feasible or economical

Chapter 3

Material and methods

This chapter describes the basic material and methods used throughout this entire research, both for the characterization and performance study.

3.1 Carbon nanotube growth

The first essential step for this entire study is to be able to grow nanotubes samples. They are grown on silicon wafer using standard thermal chemical vapor deposition (CVD) with ethylene and hydrogen as the precursor gasses.

The substrate is composed of different layers, being respectively:

- A bottom layer of single crystalline silicon substrate.
- An intermediate layer of aluminum oxide buffer, with thickness of 10nm $\pm$ 2nm.
- A top layer of iron catalyst, with thickness of 1nm $\pm$ 0.2nm.

Without the aluminum oxide buffer layer, the iron layer melts at the high temperature needed for the CVD process and diffuses into the silicon wafer, thus circumventing any growth. The presence of aluminum oxide buffer layer between the iron layer and the silicon wafer prevents this effect and allows the iron to catalyze the growth reaction at high temperatures. Aluminum oxide and iron layers are deposited on the silicon wafer by electron beam evaporation at a very low pressure of 10^{-6} Torr. In contrast to the sputtering technique, thin film deposition using electron beam evaporation technique

results in a very uniform thickness and a very low surface roughness. To align CNT in an array, a high density of catalysts on a flat surface is necessary to confine CNT growth direction (13).

This evaporation technique requires an extreme precision of ± 0.2nm in thickness onto the substrate deposition, which required multiple new calibrations over the year. During this whole year, numerous experiments had to be redone multiple times because of issues with the calibration of the electron beam evaporator. Thus obtaining wafers is a very challenging task despite their apparent theoretical simplicity.

The growth recipe had also been changed three times this year, when a check valves and filters of the furnace had to be replaced. This involves a lot of trial and errors, and tentative research, since there are so many parameters involved, it is hard to determine which one - or which set of parameters - is responsible for the bad growth. Moreover, the anchoring technique of nanotubes on PDMS (as explained in the article " *Controlled partial embedding of carbon nanotubes within flexible transparent layers*", by E. Samson (14)) and on copper tape for use in electrochemical cells have a low success rate of about 40% and 50% of the as-grown samples respectively. The anchoring process on copper tape is similar to the anchoring process on PDMS, which is described in figure 3.1, although the curing process is omitted. Once the nanotubes are anchored on the tape, the wafer is immediately removed.

The average length of the arrays used for this study is about 700 to 1000 μm.

3.2 Functionalization

Even though as-grown carbon nanotubes possess an array of unprecedented structural, physical, mechanical and electrical properties, a lot of improvement can be achieved through further functionalization. The surface chemistry tuning of the CNT was achieved through a combination of UV-ozone and vacuum pyrolysis treatments, as shown in figure 3.2.

3.2.1 Hydrophobization

Different processes can be used to produce hydrophobic nanotubes, such as dry plasma treatments or wet chemical coating. However, vacuum pyrolysis treatment was found to be the easiest way to proceed, although not the fastest. It reverses the effect of

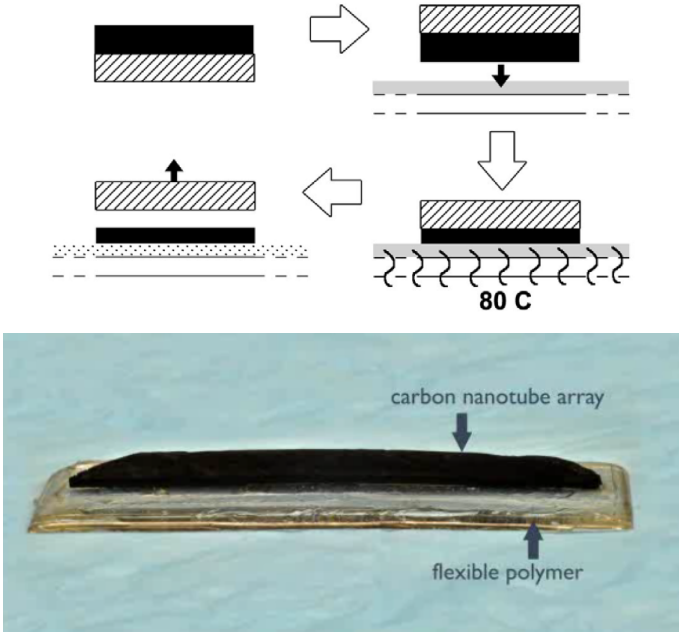

Figure 3.1: Anchoring of VANT on PDMS substrate - The dashed rectangles represent the silicon wafer, while the black rectangles depict the VANT. The grey area is the uncured PDMS, baked at 80C to solidify and allowing an easy removal of the wafer.

oxidation by removing the oxygenated groups from the surface of the nanotubes, while keeping the microscopic structure of the array intact (15).

A hydrophobic CNT array is defined as an array that has purity higher than 95% and has static contact angle for water higher than 150 °.

3.2.2 Hydrophilization

Several papers report the significant improvements achieved by making the carbon nanotubes hydrophilic, which can be made by functionalizing their surface with oxygenated functional groups, such as -COOH and -OH. Such functional groups provide hydrophilic sites on the surface of the nanotubes. Hydrogen bonds can form between the water molecules and the functional groups added to the surface of the nanotubes. (15). UV-ozone treatment was the method chosen to oxidize the nanotubes with oxygenated groups at standard room temperature and pressure. UV radiation creates defects on the caps and outer sidewall of the nanotubes, which allows ozone to oxidize these sites with oxygenated groups. The hydrophilic CNT array is defined as an array

that has been previously functionalized with oxygenated functional groups, e.g. hydroxyl groups, via oxidation process and has static contact angle for water lower than 30 °.

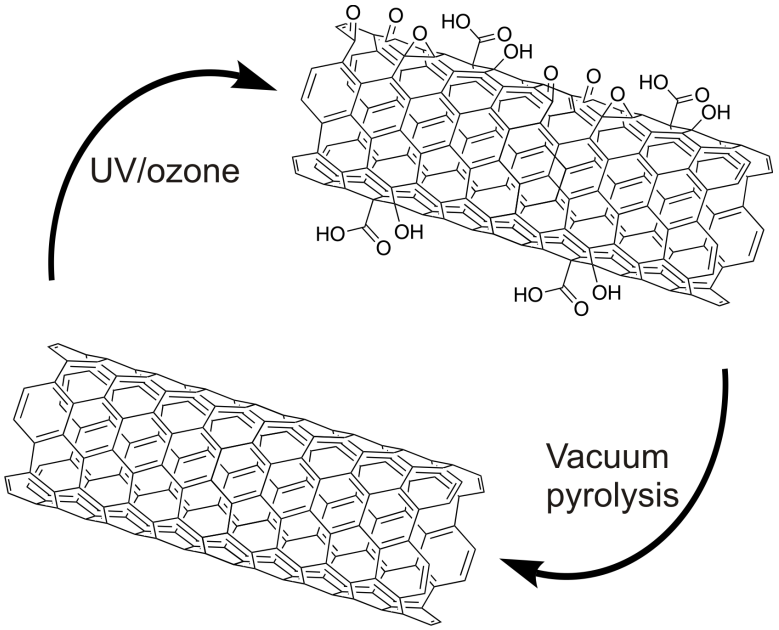

Figure 3.2: UV/ozone and vacuum pyrolysis treatments - Both are used to vary the wetting properties of CNT arrays. Oxygen adsorption occurs during UV/ozone treatment and oxygen desorption take places during vacuum pyrolysis treatment. Taken from (15)

3.3 Cyclic voltammetry

This section is greatly inspired by the article *"Cyclic voltammetry"* from Peter T. Kissinger (16).

3.3.1 Theory

Cyclic voltammetry is a widely used electrochemical characterization technique, because of its ability and effectiveness to quickly observe an electrochemical behavior over a wide potential range. This electrochemical characterization records the working electrode potential as it is cycled over time. For each cycle, this potential is varied linearly in time between a given minimum potential and a predetermined maximum potential. This gives a typical excitation signal, the triangular waveform seen on figure

3.3. The electrode potential sweeps between the two peak values set at the beginning of the experiment for a predefined number of cycles. A pair of sweeps in opposite directions - forward scan plus reverse scan - is called a cycle.

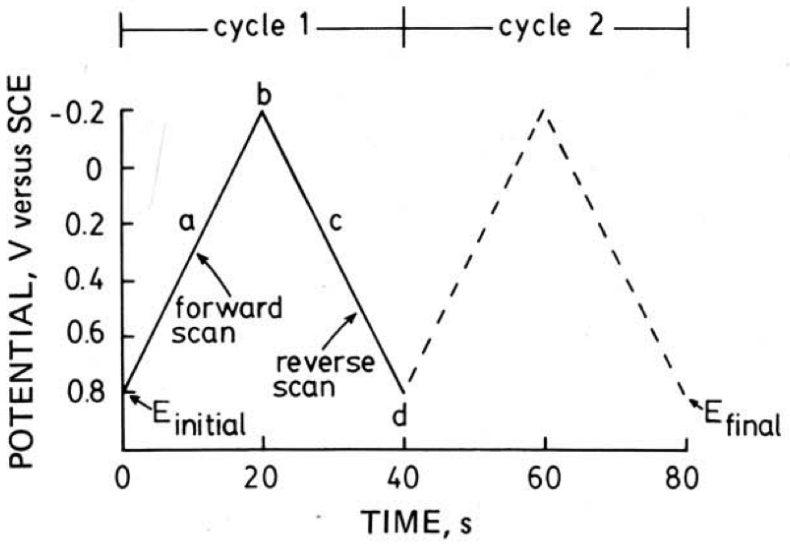

Figure 3.3: Excitation signal for cyclic voltammetry - Taken from Peter T. Kissinger's article (16)

The rate of change of potential with time is referred as the scan rate (ν), it is reflected by the slope and measured in mV/s. The voltammogram measures the current at the working electrode, as the response signal to the excitation signal in function of the voltage. Some examples can be seen on figures 4.2, 4.3 and 4.6. Since the voltage is varying linearly with time, one can think of the voltage x-axis as a time axis. The potential range is chosen accordingly to the electrolyte: in an aqueous solution, we want to avoid the electrolysis of water ($E^\circ = 1.23$V), so the maximum will be kept around 1V. As mentioned previously, the advantage of non-aqueous solution is that the potential range can be extended to nearly 3V in theory. Such a system has a higher energy density because the working voltage window is larger (17). With the increase of scan rate, the voltammogram becomes tilted. This reflects that at fast scan rates, the ohmic resistance is very prominent, thus affecting the double layer formation mechanism and the charge stored in the capacitor (18).

3.3.2 Setup

For the first half of the year, a three-electrode setup was used. The working electrode (WE) was controlled against a reference electrode (often a saturated calomel electrode, with a constant electrochemical potential), and the counter electrode (CE) was an inert platinum (Pt) electrode. When the measurement was conducted, all electrodes were immersed in the electrolyte. This setup allows studying only one electrode in isolation, without having to worry about the interference from the other electrodes. However, most of the measurements made during the last part of this project were carried out using a two-electrodes setup in a real electrochemical cell made for R&D research as depicted on figure 3.4. The WE was set to be the same material as the CE, which includes graphite, dispersed nanotubes or VANT. These electrodes were separated by a filter of polypropylene while immersed in the electrolyte.

Figure 3.4: Split Flat Cell - Split Flat Cell for R&D Battery, from MTI Corporation

3.3.3 Formulas used using the CV curves

The formula used for specific capacitance [F/g] reflects the fact that the anodic and cathodic voltammetric charges are not same (19), and thus uses the integral area of the CV curve:

$$SC = \frac{\int_{E_1}^{E_2} i(E)dE}{2(E_2 - E_1)m\nu} \tag{3.1}$$

m mass of the active material, with or without the current collector
ν scan rate [mV/s], between 1mV/s and 200 mV/s usually
E_1, E_2, initial and final voltage [V], typically [0 – 1.5V] in 1M Et_4NBF_4-PC
$\int_{E_1}^{E_2} i(E)dE$ area enclosed by the curve [mA.V]

The integral was directly calculated on the voltammogram, using the integration tool from EC-Lab.

3.4 Electrochemical Impedance Spectroscopy

The following chapter is highly based on the article by Byoung-Yong Chang and Su-Moon Park, *"Electrochemical Impedance Spectroscopy"* (20).

3.4.1 Basic knowledge

The Ohm's law defines resistance in terms of the ratio between voltage, E [V], and current, I [A]:

$$R = \frac{E}{I} \tag{3.2}$$

However, this relationship is only valid for ideal resistors, which are independent of frequency, phase, and follows the relationship 3.2 for any current and voltage. This cannot explain the behavior of more complex circuits. Impedance is hence used to replace the too simple concept of resistance. Impedance measures the capacity of a circuit to withstand a flow of current, but without the limitations listed before (frequency and phase independence, Ohm's law valid at all times).

Electrochemical impedance spectroscopy (EIS) characterizes the system response when a small periodic AC signal is applied to the electrochemical cell, at different frequencies, ranging from tens of mHz to a few MHz. It then records the emerging current passing through the cell. Analysis of the system response offers useful information about the EDLC interface, its structure and the chemical reactions that might occur. Because the excitation signal is small, a linear or pseudo-linear response can be expected, which means that at a small enough scale, the behavior appears to be linear (10). Hence, if a sinusoid potential is applied, a sinusoid with an equal frequency but phase-shifted will be observed for the response, as seen on figure **??**.

3.4.2 Analysis of the curves

EIS data is analyzed by fitting it to an equivalent electrical circuit. Such equivalent circuit can be extremely complicated, but is often composed of basics elements such as resistors and capacitors. Each element should explain the physical and electrochemical

behavior of the system or part of it. The most frequent model used in this study is described in figure 3.5, and is based on Randle's model to describe the electrochemical reactions that occur at the electrode-electrolyte interface.

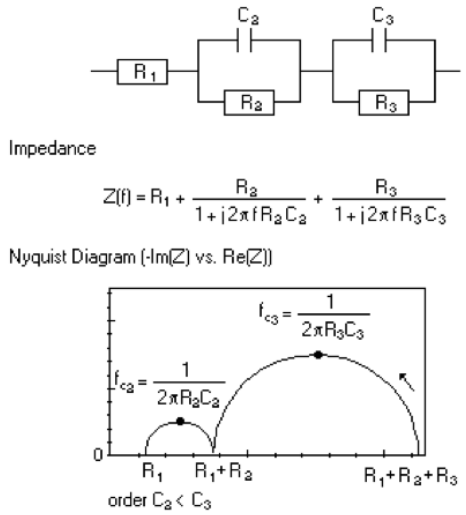

Figure 3.5: Equivalent electrical circuit

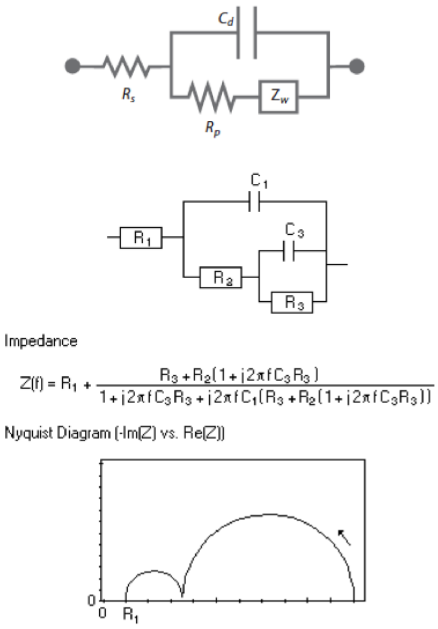

Figure 3.6: Randle's model and equivalent circuit

This circuit is an equivalent to the Randle's model shown in figure 3.6, with Z_w (explained in more details below) representing a capacitor that is in parallel with a resistor. As shown on figures 3.5 and 3.6, the R_1+C_1/(R_2+C_3/R_3) model is equivalent to the R_1+C_2/R_2+C_3/R_3 one.

- R_1 describes the cell's electrolyte resistance. This resistance depends on the ionic concentration, the type of ions involved, the temperature as well as the geometry of the electrolyte in which the current flows.

- R_2 and C_2 are the characteristic resistance and capacitance of the electrode-electrolyte interface. R_2 describes the polarization resistance across the interface, or in other words, the activation barrier for an electron transfer across the double-layer that has to be overcome (22). When an electrode is polarized, namely forced away from its value at open-circuit, electrochemical reactions occur at the

electrode surface, causing an electric current to flow. C_2 describes the capacitive behavior of the double-layer capacitance.

- Finally, the term Z_w describes the charge and mass transfers taking place at the interface, i.e. the diffusion of oxidant to the cathode.

This is summarized in figure 3.7. Specific capacitance obtained from EIS was only used to corroborate the data found from CV and charge-discharge tests; if they were in the same order of magnitude, the experiment was considered reliable. The EIS data will not be mentioned in this study

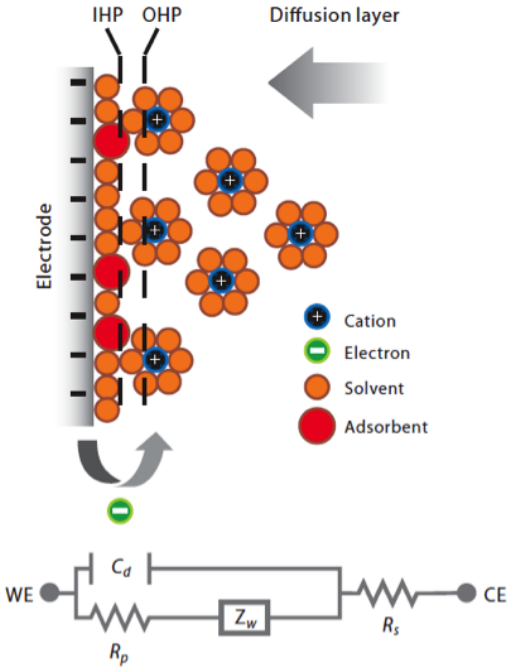

Figure 3.7: Simple electrified interface - An equivalent circuit representing each component at the interface and in the solution is also shown (20)

3.5 Field emission Scanning Electron Microscope (FESEM)

High-energy electrons from an electron gun are accelerated in a vacuum through a voltage difference of a few keV between cathode and anode. The interaction between these incident electrons and the sample produces a signal of scattered electrons that

can be recorded by detectors inside the specimen chamber (23). This output signal includes secondary electrons, back-scattered and forward-scattered electrons, and X-rays, as depicted on figure 3.8. Among these, only the secondary electrons were useful for imaging the carbon nanotubes. The detectors collect these electrons and convert them into a signal that is sent to the screen to produce the final image.

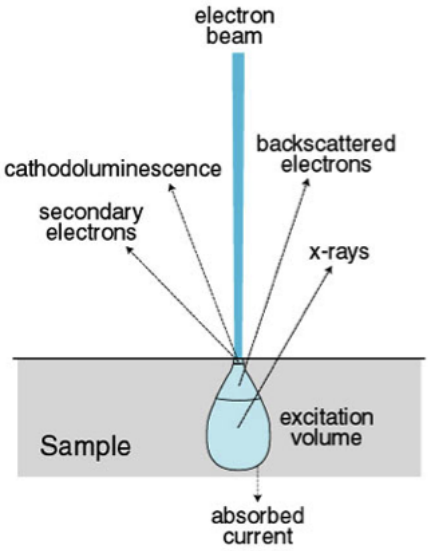

Figure 3.8: Interaction effects - A focused beam of electrons bombards the sample, and most incident electrons, rather than penetrating the sample, interact with the sample atoms and are scattered. Image taken from Northern Arizona University.

Carbon nanotubes are naturally dry, which is really important because water or any aqueous solution would vaporize inside the vacuum chamber and damage the microscope. Because the nanotubes are conductive, usually no additional preparation is needed. However, with some samples covered with amorphous carbon or embedded in PDMS, sputter-coating was used to make them conductive by coating the sample with a thin layer of metal, usually 5nm of Pt-Pd alloy. This prevents surface charging, which causes an apparent movement, distortion and artifact of the image viewed under SEM. This was a recurring problem, especially when using VANT anchored in PDMS or bad samples with a lot of amorphous carbon. Surface charging is caused by an accumulation of electrons on the surface, which build up charged regions. These deflect the incident electron probe irregularly, because the charging alters secondary electron emission and make the signal electrons unstable. A good electrical conduction ensures the removal

of excess electron easily (24).

3.6 Energy-dispersive X-ray spectroscopy (EDS)

This technique uses the SEM to bombard the sample with electrons, and decode the resulting pattern of electron reflection to generate a detailed quantification of every element involved. Some higher energy electrons replace the electrons ejected from the surface of the sample. To maintain energy balance, some energy must be released, in the form of X-rays. The X-ray spectrum is then analyzed, and decoded in function of the element from which it is released (25). This technique gives quantitative insights on the sample composition.

3.7 Galvanostatic charge-discharge

The discharge curves should be linear in the total range of potential with constant slopes to show a perfect capacitive behavior, namely, a perfect triangular shape (26).

However, this was not the case here, such that the formula

$$C = \frac{I}{dV/dt} \tag{3.3}$$

used in most papers is no longer valid, because of the inconstant slope. Therefore, a more appropriate formula is found by integrating the equation 2.1 over time:

$$\int Q dt = \int CV dt = C \int V dt - \int \left(\frac{dC}{dt} \int (V dt) \right) dt \tag{3.4}$$

Assuming once more that $\frac{dC}{dt} = 0$, we obtain:

$$\int Q dt = C \int V dt \tag{3.5}$$

Recall that:

$$I = \frac{dQ}{dt} \tag{3.6}$$

$$\int \left(\int I dt \right) dt = C \int V dt \tag{3.7}$$

With I being constant over time and Δt being the discharge time, we find:

$$\frac{1}{2} I \Delta t^2 = C \int_0^{\Delta t} V dt \Longrightarrow C = \frac{I \Delta t^2}{2 \int_0^{\Delta t} V dt} \tag{3.8}$$

$$SC = \frac{I\Delta t^2}{2m\int_0^{\Delta t} V dt} \tag{3.9}$$

This formula is used to determine the specific capacitance from the charge-discharge curves, which is then compared to the specific capacitance obtained via CV. When those values agree to each other the experiment is validated.

Chapter 4

Characterization

This chapter aims at specifying and detailing the whole system, comprised of the electrolyte and the electrodes.

4.1 Electrolytes

4.1.1 Saline solution and sulfuric acid solution

These solutions were found to give quite low specific capacitance, unstable and their cyclic voltammograms show some non-expected shapes and peaks that could not be easily explained. In addition, acid electrolytes were found to be too destructive for the carbon nanotubes.

These were abandoned quickly.

4.1.2 Aqueous solution

This part of the experiments inspired by the paper *"Flexible energy storage devices based on nanocomposite paper"*, by Pushparaj and al (27). The idea was to use a similar setup, and to compare the results obtained, and see similar results can be obtained. This would assess the suitability of our nanotubes as good electrodes for supercapacitors. A solution of 6M KOH was used. Using an operating voltage of 0.9V, the paper reports a specific capacitance of 36 F/g.

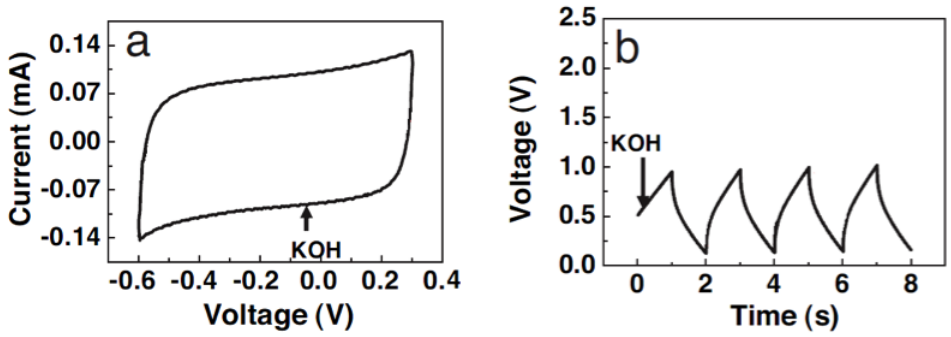

Figure 4.1: Electrochemical double-layer capacitance measurements - (a) Cyclic voltammograms and (b) Charge-discharge behavior of the nanocomposite supercapacitor devices with KOH electrolytes. The CV measurements are carried out at a scan rate of 50 mV/s at room temperature. The near-rectangular shape of the CV curves indicates good capacitive characteristics for the device. Charge-discharge behavior was measured at a constant current of 1 mA (27).

Using the same potential window, a specific capacitance of 29.7 $\pm$ 3.4 F/g was obtained for a hydrophilic sample. Even though this result is lower, the order of magnitude is comparable. In conclusion, the setup used was good and able to reproduce comparable results. Some improvements were then added and carried out with a similar setup to the one used in the paper.

4.1.3 Non aqueous solution

Specific capacitance achieved with aqueous solutions, either basic or acid, is often higher than that in organic electrolytes. Nevertheless, organic electrolytes are more widely used since they can sustain a higher operation voltage, up to 2.7-3V in symmetric systems (28), compared to only 1V in aqueous solution (7). However, some specific applications can take advantage of either solution: supercapacitors using aqueous systems are appropriately designed as power sources for pulsed applications, whereas non aqueous supercapacitors are designed for high energy applications (17)

Various non-aqueous electrolytes were investigated, as listed below:

- Iodine-iodide (I^-/I_3^-): because it is a very strong oxidizing agent, corroding metals especially in the presence of water and oxygen, and because the results were extremely bad, it was quickly abandoned. The initial idea was to use this electrolyte for the energy generation project, but the deleterious and detrimental

	Aqueous	Organic
Voltage per cell	Maximum = 1V	Maximum = 2.7V
Manufacture	Easy	Difficult
Cost	Low price	High price
Leakage current	Quick stabilization	Long stabilization needed
Environmentally friendly	Green product	Not a green product

Table 4.1: Comparison of aqueous and organic electrolytes - From Cellergy Technology - Supercapacitor

effect of iodine-iodide on carbon hindered further use of this electrolyte. It was also the beginning of the re-orientation of the project from energy generation toward energy storage, since the carbon nanotubes needed milder electrolytes.

- Tetrabutylammonium tetrafluoroborate in propylene carbonate (But_4NBF_4/PC)
- Tetrabutylphosphonium tetrafluoroborate in propylene carbonate (But_4PBF_4/PC)
- Tetraethylammonium tetrafluoroborate in propylene carbonate (Et_4NBF_4/PC)

These three electrolytes salts were dissolved in propylene carbonate (PC), at a concentration of 1M for both Et_4NBF_4 and But_4NBF_4, which is reported to be an optimal concentration that gives the maximum conductivity and the best results (29). In the case of But_4PBF_4, 0.1M was used due to availability issues of the salt. Ethylene carbonate has a higher dielectric constant than propylene carbonate up to 87.2 at 25 °C against only 64.6 for propylene carbonate. Ethylene carbonate has a calculated dipole moment of 4.87 Debye (30, 31). Despite these very promising characteristics, EC is hard to manipulate: it has a melting temperature higher than the standard room temperature such that it needs to be heated for use as a solvent, and has to be kept away from humid air because it is hygroscopic. The results were slightly better than that with propylene carbonate, with an improvement in the order of 10%. Nevertheless, the slight increase was not worth the trouble with the handling and manipulation, and the rest of the experiments were conducted using propylene carbonate.

The table 4.1 summarizes the different advantages and drawbacks of both organic and aqueous electrolytes.

4.1.4 Choice of liquid solution over gels and polymers

Many studies have reported the use of polymers or gels instead of liquid electrolytes, with overall great results. However, some fundamental drawbacks of these materials, such as their higher resistivity and their poor contact with electrodes have limited their use in supercapacitors (32, 33, 34).

Hence, liquid electrolytes were preferred for this study.

4.2 Capacitive behavior

VANT electrodes were compared to graphite electrodes to show that the former would yield higher specific capacitance. This comparison is in agreement with previously reported studies (35).

4.2.1 Graphite voltammogram

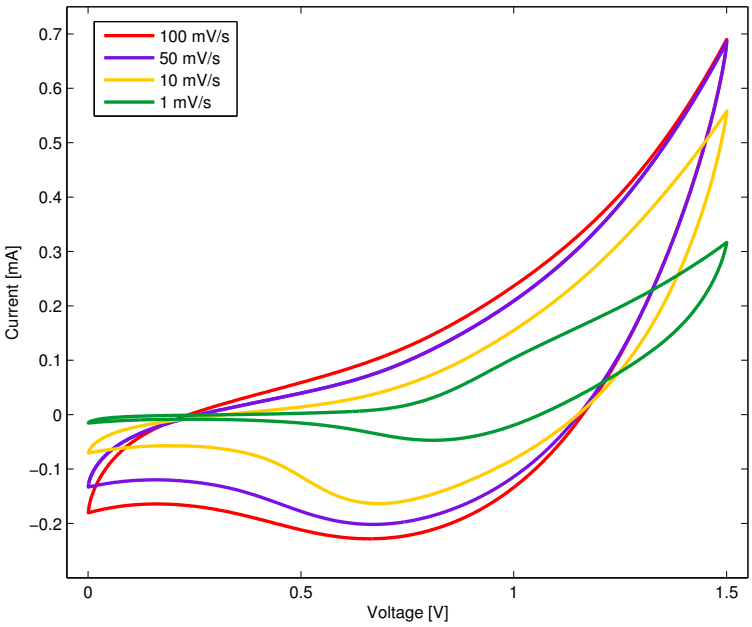

Figure 4.2: Voltammograms of graphite - Experiment realized in 1M Et_4NBF_4-PC, at different scan rates

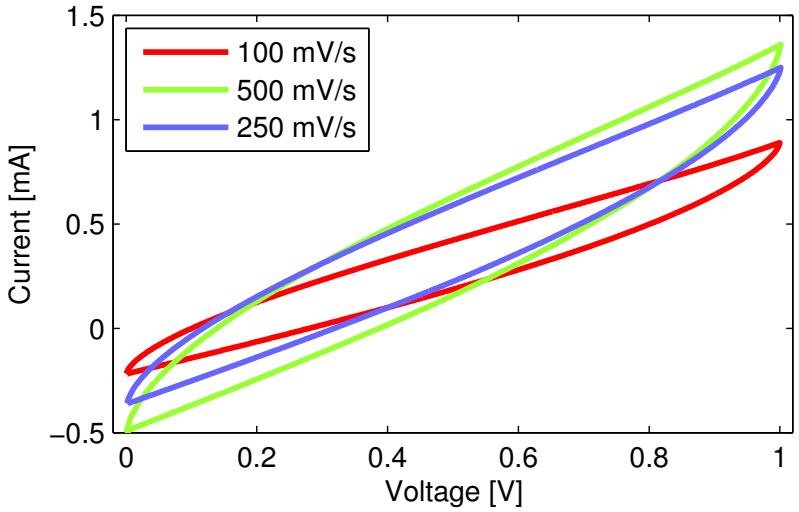

Figure 4.3: Voltammograms using a graphite electrode - Experiment realized in 1M Et_4NBF_4-PC, with a smaller voltage window

First, graphite was investigated as a carbon-based material with a high surface area. Graphite electrodes were used in 1M Et_4NBF_4-PC electrolyte. The capacitive behavior of the graphite based double-layer capacitor is studied through cyclic voltammetry at different scan rates ranging from 1mV/s to 100mV/s, as seen on figure 4.2.

The voltammogram clearly shows that the graphite is not a good choice for the electrode, and cannot be used at a voltage range of 0-1.5V, since an elbow is clearly distinguishable around 0.8V. A much better voltammogram was obtained if the voltage range is limited to 0-1V, as seen on figure 4.3. Note that the tilted voltammogram is due to high scan rates. The graphite voltammogram shows narrow loops with a large oblique angle around 0.8V,a typical behavior for an electrode with a large electrical resistance (36). This finding further supports the idea of graphite as a poor electrode material despite of its relatively high conductivity.

Interestingly, the graphite electrode voltammogram is nearly independent of scan rate for scan rates higher than 50 mV/s. A possible explanation for this behavior is that the size of the diffusion layer is more or less constant for scan rates higher than 25 mV/s, and we can suppose this is the minimum diffusion layer size possible since slower scan rates tend to have larger diffusion layers.

A very similar behavior, in term of both specific capacitance value and voltammo-

gram, was observed for dispersed nanotubes. Some SEM images of dispersed nanotubes and graphite are presented in figures 4.4 and 4.5 respectively.

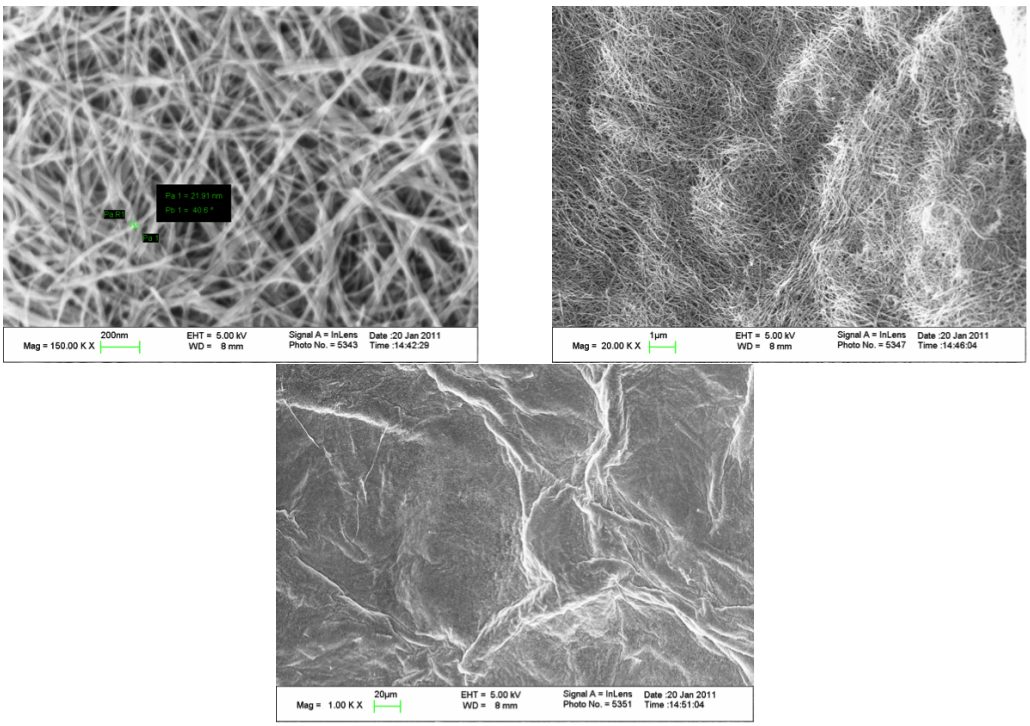

Figure 4.4: SEM images of dispersed nanotubes at different magnifications

The dispersed nanotubes presented in figure 4.4 show the characteristic tubes, entangled and twisted. The effective surface area available is slightly higher than that of the graphite layer displayed in figure 4.5.

4.2.2 VANT voltammogram

After investigating the properties of graphite-based electrodes, a similar study was conducted with VANT, and the capacitive behavior of a VANT based double-layer capacitor was recorded in figure 4.6. The scan rates were chosen between 10mV/s and 100mV/s. A good rectangular and symmetric shape is exhibited over a large range of scan rates and in accordance to the rectangular shape expected in theoretical ideal capacitors. The charge and discharge processes are very fast at the interface between the VANT and electrolyte, and the voltammogram is perfectly featureless, confirming the usefulness of VANT for supercapacitors. The featureless voltammogram probably

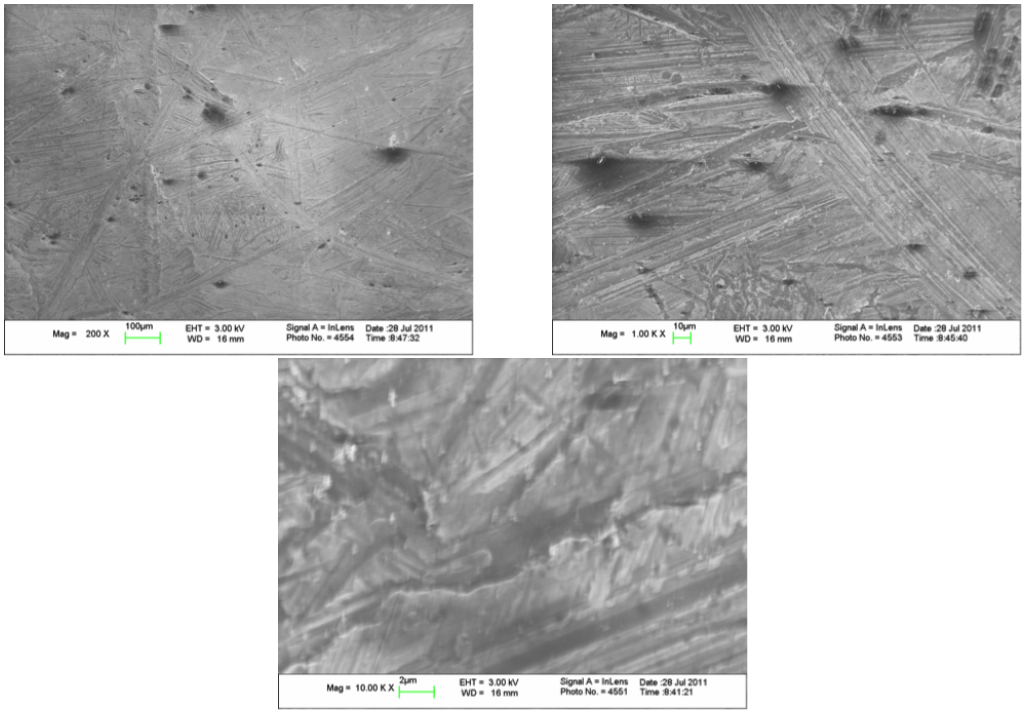

Figure 4.5: SEM images of graphite at different magnifications

results from the atomic structure variations of the nanotubes. Recall that the electronic properties of the nanotubes are extremely sensitive to changes in length, diameter, helicity of the carbon hexagon rings on the walls, or chirality (Armchair or Zigzag). Therefore, the featureless voltammogram might be an average of multiple closely spaced peaks, each one being the signature of a single electron transfer into one single tube (37).

Characterization via SEM images demonstrates that the VANT are densely packed. A quick density measurement of the VANT gave values somewhere between 0.007 and 0.013g/cm^3. Therefore, a density of 0.01 g/cm^3 is assumed. It is important to notice that high magnification reveals that the nanotubes are not perfectly straight, but rather curly and entangled at the nanometer scale (figure 4.7). A low contact resistance and a good capacitive behavior are assumed. Indeed, no significant difference (in terms of specific capacitance, resistance and voltammogram shape) appeared between bare samples and samples coated with metal, in an attempt to obtain a better contact between the sample and the copper tape. Pt-Pd alloy coats the nanotubes conformally, while Ag creates a distinct layer of metal. An increase in specific capacitance of less than

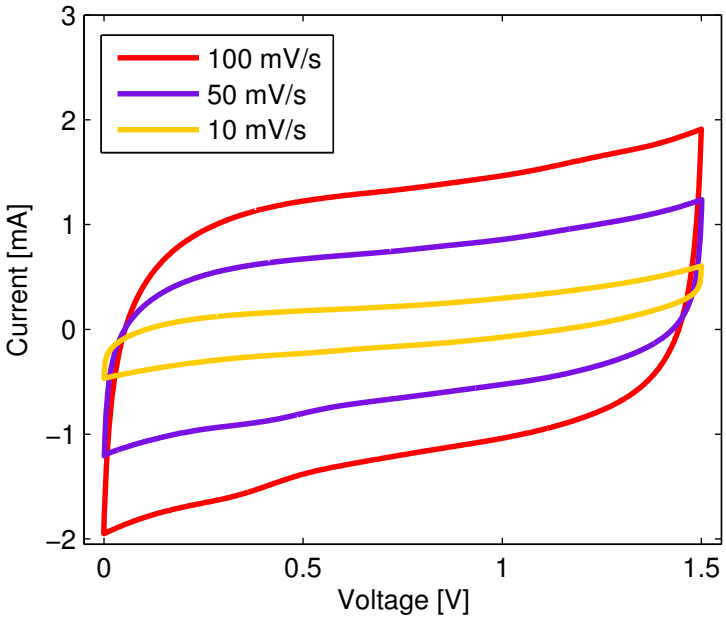

Figure 4.6: Voltammograms for a setup with VANT electrodes - Experiment realized in 1M Et_4NBF_4-PC for different scan rates

3% was observed in sample coated with 50 nm Pt-Pd, and an increase of 5% obtained by samples coated with 50nm Pt-Pd and 50nm Ag. Therefore a metal coating was considered unnecessary. This finding is encouraging since noble metals are expensive.

4.3 Relationship with scan rate

The values of specific capacitance obtained with graphite-based electrodes in function of the scan rate are summarized in the figure 4.8 below. They are low compared to that obtained with the VANT electrodes. Such low values of specific capacitance are the result of a much smaller surface area available, because only the top layer of graphite is accessible by the electrolyte. Figure 4.9 shows the relationship between specific capacitance and scan rate for VANT.

It is interesting to highlight that in both cases the behavior of the specific capacitance as a function of the scan rate follows a power law. But unlike graphite, VANT based electrode offers a very large surface area, and thus gives rise to higher specific capacitance. At lower scan rate, the specific capacitance is higher, indicating little

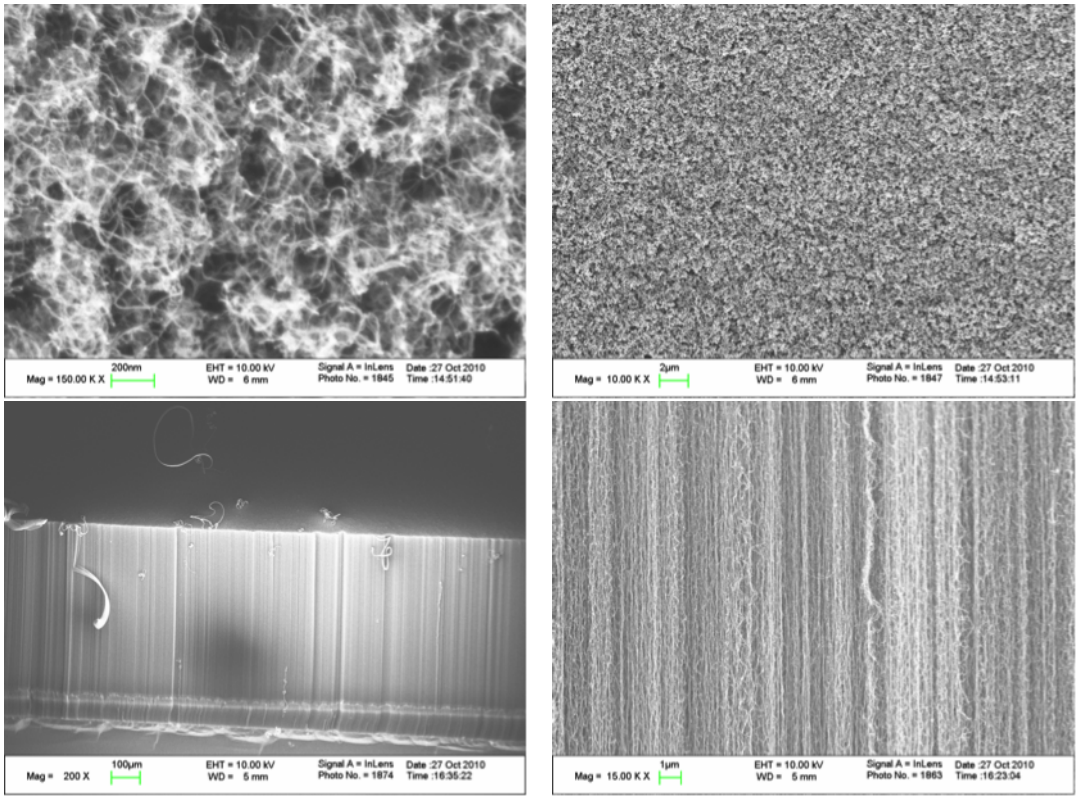

Figure 4.7: SEM images of VANT (a) Close up at 150 KX (b) Wider view at 10KX (c) 60 angle at 200X to see the height of the nanotube array (d) 60 angle highlighting the fact that the nanotubes are indeed vertically-aligned, but not completely straight at higher magnification

ionic transport limitations (38). An opposite behavior is expected at higher scan rates, where the ionic transport is slower and thus reducing the specific capacitance. A behavior that is extremely dependent of the voltage scan rate indicates some losses due to internal resistance. One of the main factors contributing to the internal losses is a high concentration of the electrolyte. At very high concentration, the electrolyte ions cannot be fully ionized, because there are not enough solvent molecules, so the current is not carried at its maximum efficiency. On the other hand, a higher concentration of electrolyte allows an increase in the specific capacitance. Hence an optimum balance between a high specific capacitance and a low resistance has to be found.

Graphite, as an allotrope of carbon with sp2 hybridization, shares a lot of common properties with carbon nanotubes, including good electrical conductivity. However, the

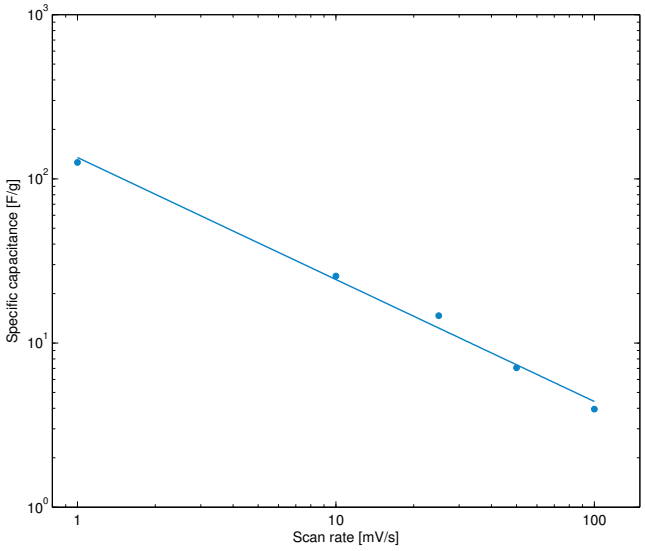

Figure 4.8: Log-log plot of relationship between the specific capacitance and the scan rate for electrodes made of graphite - A power relationship for electrodes made of graphite in 1M Et_4NBF_4-PC electrolyte holds. The following regression equation is found: $SC \simeq 130 \left(\frac{dV}{dt}\right)^{-3/4}$.

specific capacitance obtained when graphite is used as the electrode yields considerably lower specific capacitance, namely 3 to 5 times lower for the same scan rate than what can be achieved with VANT, as can be seen in figure 4.8 and 4.9.

The specific capacitance (SC, in F/g) is linked to the scan rate (ν, in mV/s) via the empirical formula:

$$SC \approx \alpha \left(\frac{dV}{dt}\right)^{\beta} \tag{4.1}$$

Where α and β for the graphite-based electrode are found to be 130 and -3/4 respectively. In the case of VANT-based electrode, α and β are found to be 310 and -3/5 respectively.

My hypotheses is that the curves obtained with additional data will tend toward a similar relationship as defined in equation 4.1, with only the α-term different - probably by a factor two to three, depending on whether graphite or VANT is analyzed. The β-term on the other hand is probably going to be similar, around -3/4.

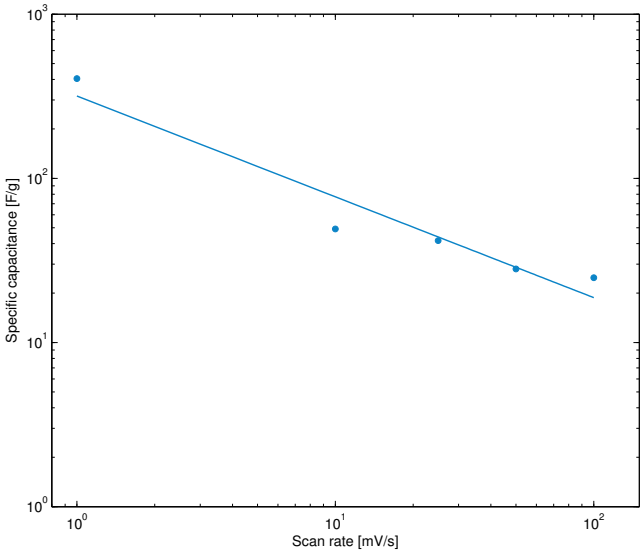

Figure 4.9: Log-log plot of relationship between the specific capacitance and the scan rate for VANT electrode - A power relationship for electrodes made of VANTs in 1M Et_4NBF_4 - PC electrolyte holds. The following regression equation is found: $SC \simeq 310 \left(\frac{dV}{dt}\right)^{-3/5}$

Chapter 5

Performance evaluation

This chapter presents the results obtained using the previously characterized samples. Different improvements and ameliorations are explored and discussed. In particular, the efficiency of the device is analyzed through its power and energy efficiencies, and lifetime.

5.1 Functionalization

In agreement to some published and studies (39, 40),the specific capacitance of a VANT-based electrode in an aqueous solution can be significantly increased by the addition of hydroxyl and carboxyl groups to the electrode. These groups increase the number of contact sites between the electrode and the electrolyte ions that leads to the increase of the global charge transfer between the electrode and electrolyte. For any polar solution, a functionalized hydrophilic VANT sample should give a higher specific capacitance due to a higher proton transfer between water and the VANT.

A 1M Et_4NBF_4 - PC solution was as an electrolyte to compare the effect of surface functionalization on both VANT array electrode and graphite electrode. The result was then compared to the literatures. Figure 5.1 summarizes these findings. A quick comparison of the performance of graphite and VANT shows that the specific capacitance of the VANT electrodes is two to three times higher than that obtained with graphite electrodes. The specific capacitance of the graphite electrode is about 20 F/g whereas

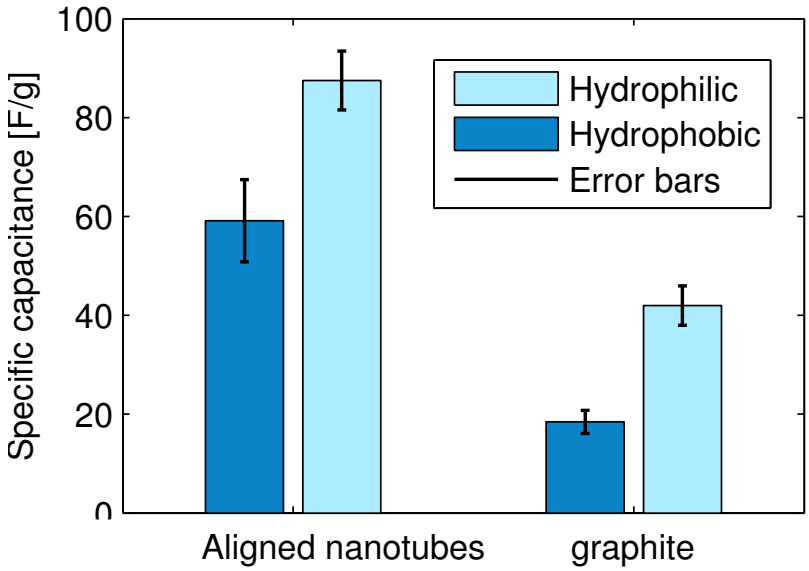

Figure 5.1: Surface functionalization - Specific capacitance of the vertically-aligned CNT array electrodes in 1M Et_4NBF_4 - PC is extremely higher than that of the graphite when both of them are functionalized, at 25 mV/s.

the specific capacitance of the hydrophobic VANT electrode is about 60 F/g. On the other hand, an increase of specific capacitance from 42 F/g for a hydrophilic graphite electrode to nearly 90 F/g for a hydrophilic VANT array electrode was observed. These findings agree with a recently reported study (35), confirming the importance of structurally aligning carbon nanotubes in the direction of ion diffusion as a way to increase the specific capacity. Such alignment leads to both an increase of the surface area available, because the electrolyte ions can access more easily and freely the sidewall of the nanotubes, and a diminution in the overall resistance of the electrode. EIS experiments were carried out to verify such behavior where a resistance of $\sim 10\,\mathrm{k\Omega} \pm 0.3\mathrm{k\Omega}$ for graphite was measured, while only $\sim 1.5\,\mathrm{k\Omega} \pm 0.1\mathrm{k\Omega}$ was measured for VANT, which is nearly an order of magnitude lower.

Different electrolytes were also investigated. First of all, aqueous solutions were explored. In an aqueous acid solution (1M H_2SO_4), the specific capacitance increases from $16 \pm 1\,\mathrm{F/g}$ to $51 \pm 2.1\,\mathrm{F/g}$ once VANT or equivalent to an increase of $\sim 320\%$ when the hydrophilic VANT are used as electrodes. Similar behavior was also observed in 6M KOH, where the specific capacitance increases from $1 \pm 0.3\,\mathrm{F/g}$ to $29 \pm 2.5\,\mathrm{F/g}$

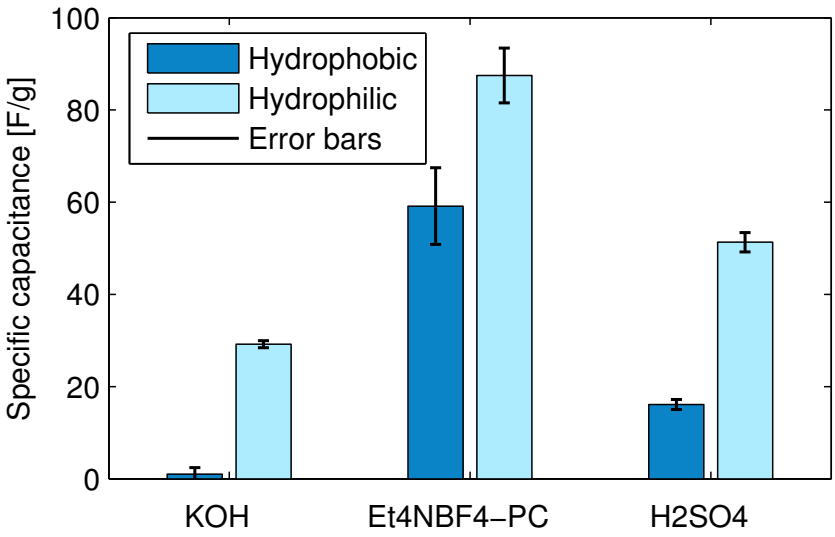

Figure 5.2: Electrolyte comparison - Specific capacitance of the vertically aligned CNT array electrodes in both aqueous (6M KOH) and non-aqueous (1M Et_4NBF_4 - PC) solution, measured at 25 mV/s.

once the VANT are functionalized, as shown on figure 5.2.

The next logical step to follow up this experiment was to investigate the effect of surface functionalization of VANT electrodes in a non-aqueous solution. As a first hypothesis, it seemed reasonable to see a difference between aqueous and non-aqueous solutions. In other words, it was expected that in a non-polar solution, the addition of hydroxyl groups on VANT would decrease the electrolyte accessibility to the entire surface area available on the nanotubes, and thus decreased the specific capacitance. This idea was further explored using a 1M Et_4NBF_4-PC electrolyte. This solution is not soluble in water although both PC and Et_4NBF_4 are highly soluble in water. Both PC and water are indeed polar solvents. Et_4NBF_4 is also soluble in water as an ionic solute in a polar solvent. However, unlike water, PC is an aprotic solvent, i.e. it does not donate protons so there is no possible interaction with the hydroxyl functional groups that were attached to the VANT. Therefore, the first logical idea was to defunctionalize the VANT such that they would not have any -OH terminal group, and making them hydrophobic. Although this idea was thought to yield higher specific capacitance, the experimental results showed the contrary. When a polar non-aqueous solution was used as the electrolyte, the functionalized VANT gave a way higher specific capacitance than

the non functionalized VANT, as seen on figure 5.2. This finding disproves the initial hypothesis made.

This early hypothesis was proven to be wrong since not all parameters were taken into consideration. Indeed, the critical factor responsible for the increase in specific capacitance was not about the fact that the solution was aqueous or not, but whether it was polar or not. The acidic and basic solutions used in this study are highly polar, as part of their Arrhenius definitions. PC is also highly polar, with a very high molecular dipole moment of nearly 5 Debye, as well as a very high dielectric constant of 64. We can suppose its high polarity creates a very effective solvation shell around Et_4N^+ ions, thus creating a very conductive electrolyte. The specific capacitance of the hydrophobic electrodes in 1M Et_4NBF_4-PC was measured to be below 60 F/g, which is significantly lower than the specific capacitance of the hydrophilic electrodes, measured to be nearly 90 F/g. This 50% increase of specific capacitance is clearly seen on figure 5.2.

So in conclusion, in both aprotic polar and protic polar solutions, an increase in hydrophilicity of the electrodes leads to an increase in specific capacitance.

As a comparison, a recent article gives a specific capacitance of 83 F/g using the same 1M Et_4NBF_4-PC electrolyte and VANT arrays electrode (41). This finding is in the same order of magnitude as what was found in this current study when using the hydrophilic CNT array electrodes (88 F/g). While encouraging, this finding is much smaller compared to another recent finding, where an extremely higher specific capacitance up to 135 F/g was achieved (42). Such high specific capacitance was achieved using either $LiBF_4$ in ethylene carbonate/diethyl carbonate as the electrolyte, and electrochemical lithium insertion into the nanotubular carbon host, or 6M KOH.

The results obtained in this study with 6M KOH were extremely lower than those reported in the above mentioned article, which may probably be attributed to a different quality of nanotubes. It was found that the VANT samples used in this study got damaged quite easily by a high concentration of basic solution, thus lowering the overall performance. Presumably a different growth recipes or growth techniques may give better nanotubes that are able to resist such a strong electrolyte.

5.2 Energy density and power density

While the specific capacitance is a good indication of the energy storage capability of a capacitor, energy density and power density are commonly used as standard normalized values.

The power density represents how much power the device can supply, while the energy density corresponds to how long the device can supply the power. Power and energy are respectively defined as follows:

$$P = CV\frac{dV}{dt} \tag{5.1}$$

$$E = \frac{1}{2}CV^2 \tag{5.2}$$

The power density (P_D) and energy density (E_D) are easily deduced by dividing by the mass of the active material (VANT) with or without including the mass of the current collector:

$$P_D = \frac{CV\frac{dV}{dt}}{m} \tag{5.3}$$

$$E_D = \frac{1}{2}\frac{CV^2}{m} \tag{5.4}$$

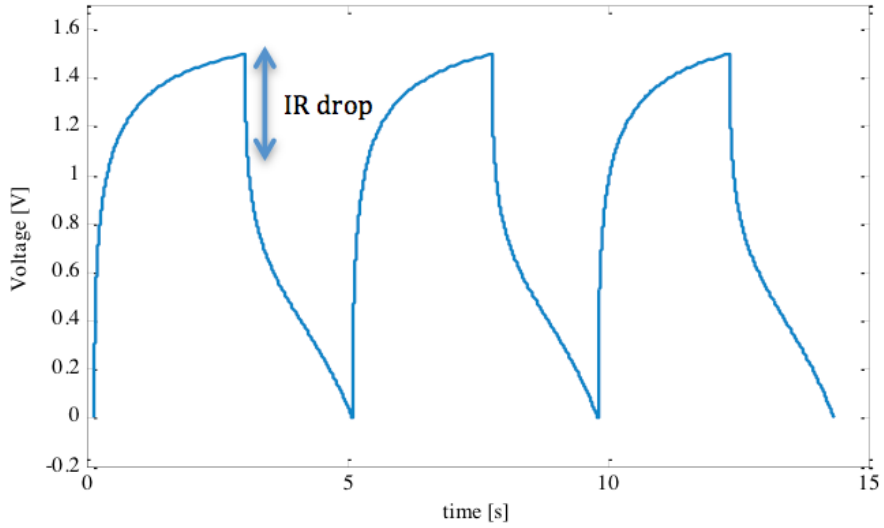

Figure 5.3: Charge-discharge curves - VANTs, for a voltage window of [0-1.5V]

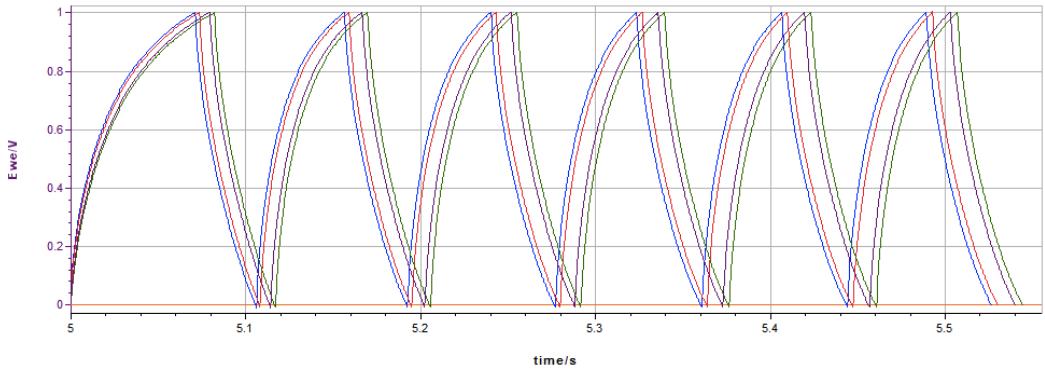

Figure 5.4: Charge-discharge curves for a smaller potential window - Use of VANT electrodes, for a voltage window of [0-1V]

The charge-discharge curves for the first three cycles are presented on figure 5.3. The most striking feature that needs to be mentioned is the non-linear and non-triangular shape, with a big drop at the beginning of the discharge period (see the ohmic drop on figure 5.3). This ohmic drop is common with dissipative systems.

A much better shape of charge-discharge curve can be achieved if the potential window is reduced to [0-1V], as seen on figure 5.4, even though it is still not perfectly triangular as expected. Since the electrolyte used for this particular experiment was an organic electrolyte, such a small potential window seemed peculiar and was unexpected. Different explanations can be found for such behavior:

- Contamination with water, which explains why the potential window cannot go past 1V. Recall the standard potential of the water electrolysis cell is -1.23 V at 25 °C at pH 0
- Other contamination with parts from the setup (maybe from the PTFE magnetic stirrer bar employed for stirring the electrolyte).
- A chemical reaction between the glue in the copper tape and the electrolyte.
- A chemical reaction between the amorphous carbon from the samples and the electrolyte.

Each of these hypotheses was thoroughly checked to discover the origin of the problem.

1) Experiment to verify if there was a contamination with water

The potential window was progressively increased from [0-1V] to [0-2V], for different current charge. The results obtained for different current charges are summarized on table 5.1. If there was a contamination with water, the increase of a potential window to [0-2V] should show a significant difference, since the standard potential of the water electrolysis cell is -1.23V. No significant difference was observed, so water is not the origin of the problem.

2) Other contamination

Different experiments were carried out by isolating every part from the setup that may induce a chemical reaction. No difference was seen when the Teflon ring, the O-rings inside the electrochemical cell and the electrolyte were replaced with the new ones.

The carbon tape cannot be held responsible since it was used before without yielding this kind of chemical reaction.

3) Conclusion

The only remaining possibility is that there is an issue with the growth itself (defective furnace) or with the deposition of Al_2O_3/Fe on the wafer. Both the furnace and the electron beam evaporator have encountered some issues during the course of this study.

Further exploration revealed that the electron beam evaporator had been contaminated where some unknown metals were deposited on the wafer when the silicon wafer was coated with iron and aluminium oxide. Such contamination inhibits the growth of the nanotubes such that the length of the array is shorter than expected and achieved before and the nanotubes are covered with amorphous carbon. This explains the inexplicable shape of the charge-discharge.

The specific capacitance in function of the discharge current is shown in figure 5.5. The values for specific capacitance were found using the formula 3.9 shown in section 3.7. If only the active material is considered, the maximum specific capacitance was found to be $\sim$1 kF/g with a discharge current density of 4.5 A/g. A comparable specific capacitance of nearly 1000 F/g can be found with cyclic voltammetry with a very low scan rate (around 0.15 mV/s) assuming the relation 4.1 holds for low voltages

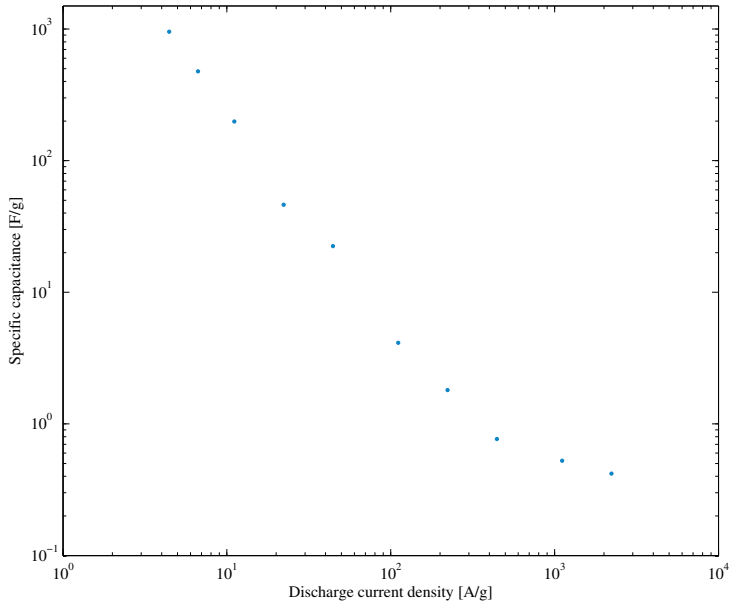

Figure 5.5: Specific capacitances of the nanotube array electrodes as a function of discharge current density - For current densities below 1000A/g, a power law holds

as well. Such a very slow scan rate regime was not explored in this study. When taking into account the mass of the overall device including the filter and current collector, the maximum specific capacitance achieved is 0.8 F/g for a discharge current of 3.5 mA/g.

The specific capacitance decreases as increases the discharge current as reported by previous studies (18). The specific capacitance decreases from 0.95 kF/g to 0.4 F/g as the current discharge increases from 4.5 A/g to 2.5 kA/g. This behavior can mainly be explained by the lower ionic mobility due to diffusion (35). One can highlight that the specific capacitance decreases of around two orders of magnitude when the discharge current is increased by only one order of magnitude. When the discharge current is low enough, meaning below ∼1000A/g, a power law holds.

Using the results from the experiments using 1M Et_4NBF_4 electrolyte, the maximum energy density was found to be 21 Wh/kg at power density of ∼1.1 kW/kg for a hydrophilic electrode, and the maximum power density was found to be ∼22 kW/kg at energy density of ∼2 Wh/kg for a hydrophobic sample as seen on figure 5.6. This

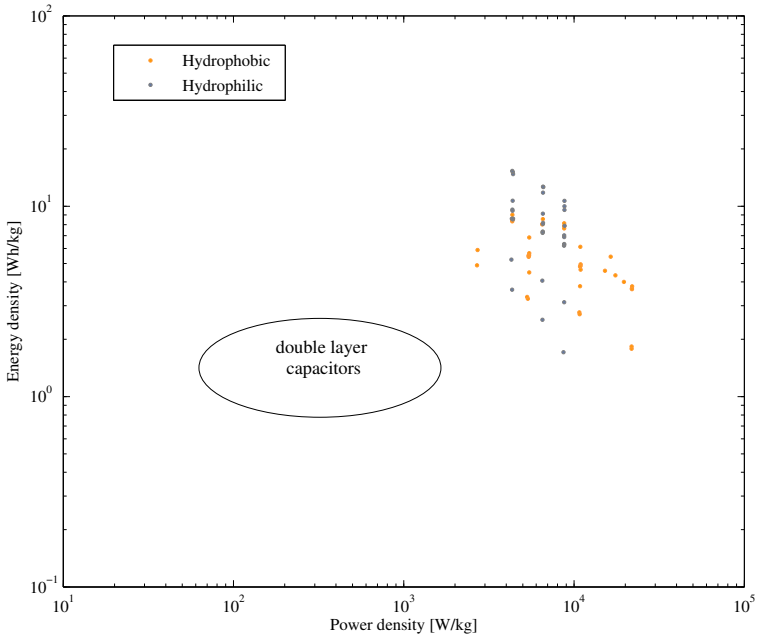

Figure 5.6: Ragone plot - Energy density in function of power density

plot was made using only the mass of the active material.

It is interesting to highlight the different behaviors between the functionalized VANT electrode and the non functionalized one. When hydrophilic VANT electrode is used, the obtained specific capacitance is higher, as already shown in figure 5.2. As a result, the energy density of the hydrophilic samples is twice of that of the hydrophobic electrodes. On the contrary, the power density is higher by a factor two when using hydrophobic VANT array electrodes. PC here is used as a polar solvent (43) so the interaction between the non-polar hydrophobic surface of the VANT array and the polar electrolyte generates a very strong repulsion. When a current is applied, the induced repulsion enhances the charge transport, and hence the power is increased. On the other hand, when hydrophilic CNT arrays electrode are in contact with polar electrolyte, dipole-dipole interactions are created between the ions and the nanotubes, which must then be broken, resulting in a lower charge flow and thus lower power. These values of power density and energy density were calculated using only the weight of the active material, i.e. the VANT. However, if the weight of the overall components including the current collector and filter is taken into account, a maximum energy density of 0.17

Wh/kg at power density of 9 W/kg, and a maximum power density of 175 W/kg at energy density of 15 mWh/kg are obtained. Even though these numbers are not that attractive, one has to remember that copper is used as a current collector. Copper is extremely heavy, about two orders of magnitude heavier than the VANT. This major drawback could be overcome by using other lighter weight current collectors, as already proposed by numerous other groups facing the same issue (44).

5.3 Lifetime

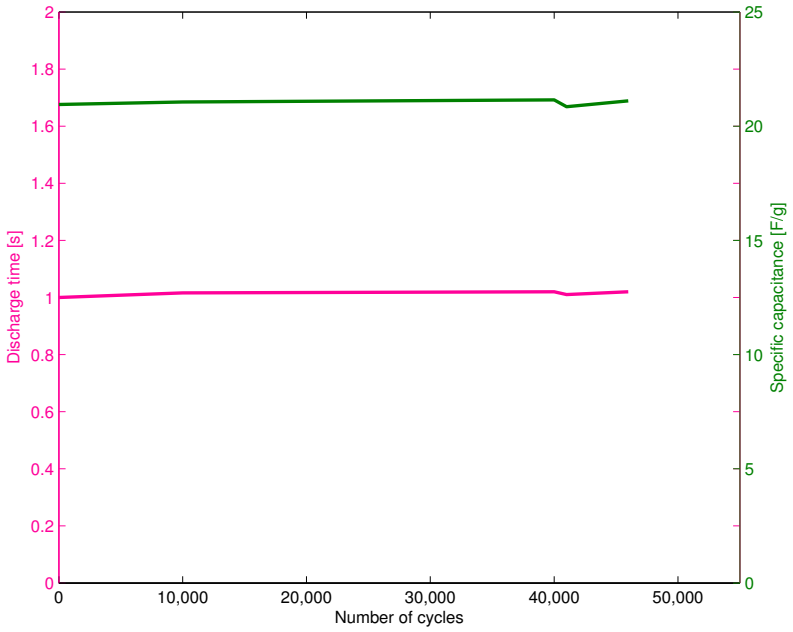

Figure 5.7: Evolution of specific capacitance in function of cycles - The storage ability is kept for tens of thousands of cycles

The lifetime of VANT based capacitor is extremely long, with nearly no change in specific capacitance after being run for more than hundreds of thousands of cycles. The figure 5.7 shows the last fifty thousand cycles, with no change in the specific capacitance as well as in the discharge time. A couple of thousands cycles were needed to reach the maximum value of specific capacitance, as further explained in the next part (see chapter 6.2). The experiment was stopped after ∼130 000 cycles, not because of the

degradation of the electrodes but because of time consideration. Indeed, it took several days to run that many cycles. More extended work to find the full lifetime has to be done. However, this work could not be achieved if the time is limited. A voltammogram after the lifetime experiment was stopped at 100 000 cycles is shown in figure 5.8, and neither any degradation of the electrodes nor any diminution in the capability to store the energy is observed.

These findings are extremely encouraging, although the energy density is smaller in comparison to an earlier reported study using nanotubes and silver nanowire films on a highly conductive paper in a lithium-based electrolyte ($LiPF_6$ in ethylene carbonate) (45). However, these quality materials are extremely expensive and present some inherent danger due to their reactive nature. The working voltage range chosen here is 0-1.5V, which allows for a longer lifetime at the cost of a lower energy density.

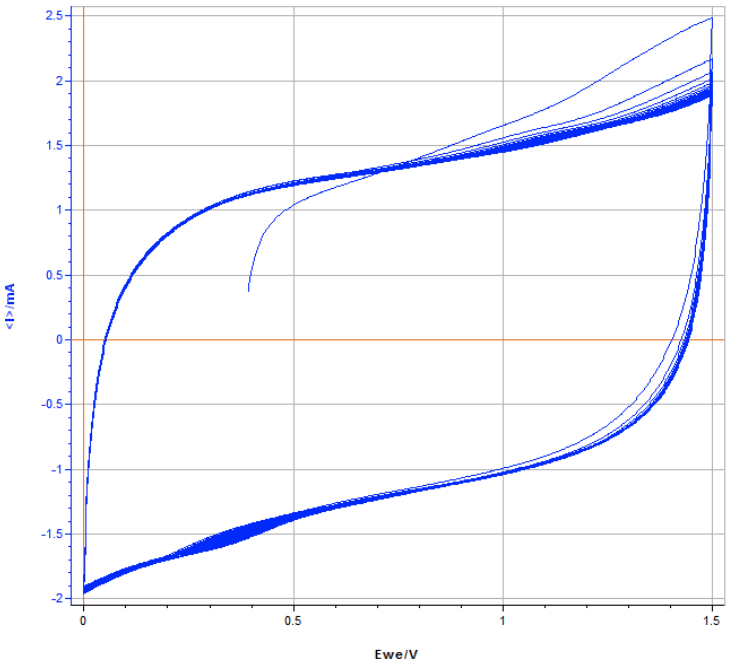

Figure 5.8: Voltammogram after 100 000 charge-discharge cycles - The 50 cycles are recorded at 100mV/s and are very stable over time, proof they can still perfectly store the energy. Note that a few cycles are needed to reach the steady state, starting from the open circuit current.

5.4 Relation to oxygen-carbon ratio

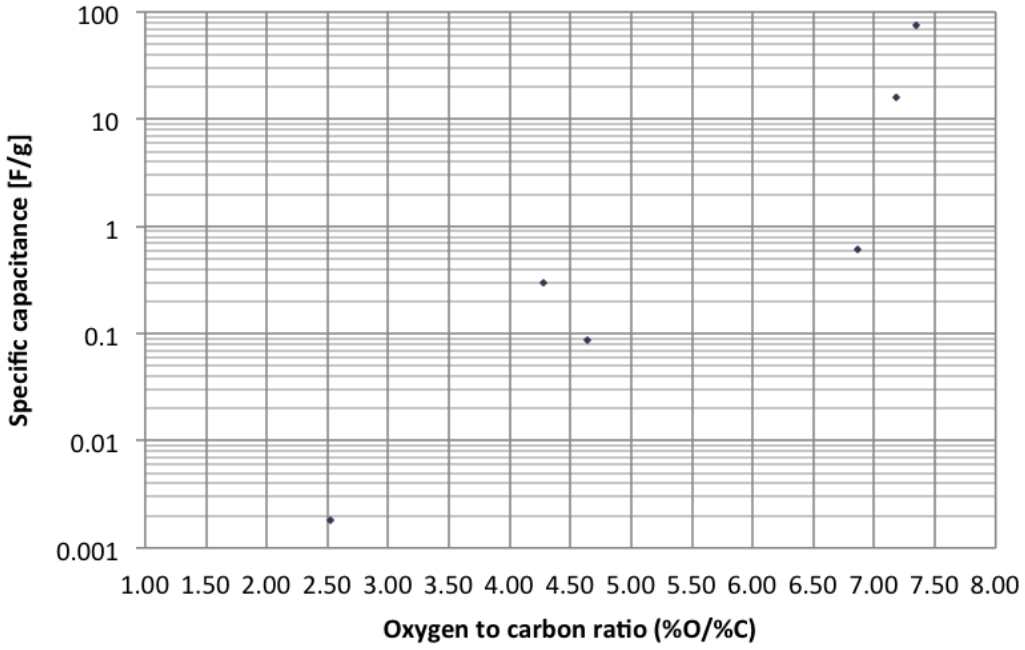

Figure 5.9: Evolution of the specific capacitance in function of the hydrophilicity - An increase of five orders of magnitude in specific capacitance is presented over an increase of 2.5% to 7.5% oxygen. A solution of in 6M KOH is used.

The increase of specific capacitance in function of the degree of functionalization, or in other words, the oxygen-carbon ratio, was investigated as well. This investigation shows that the performance of a carbon-based supercapacitor can be determined by its oxygen-to-carbon ratio.

An augmentation of nearly five orders of magnitude in the specific capacitance when the nanotubes are functionalized with hydroxyl groups can be clearly seen, thence increasing the oxygen-carbon ratio, as seen in figure 5.9. While this behavior was assessed in an aqueous electrolyte (6M KOH), the behavior is expected to be similar with an organic solvent. The experiment was repeated in 1M Et_4NBF_4 electrolyte, but did not succeed because of issues with the samples.

Table 5.1: Influence of the voltage window on the charge-discharge curves

Voltage window [V]	Current charge [mA]	Time to complete 5000 cycles [s]	Steady-state discharge time [s]	Plot of the first cycles
[0-1V]	10	75.31	0.005	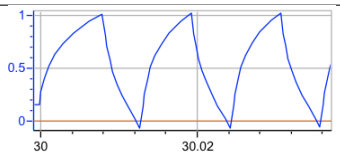
	50	9.99	0.001	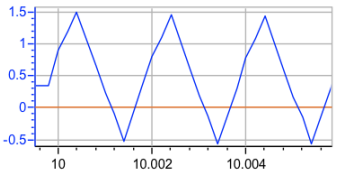
	100	8.00	<0.001 (resolution limit)	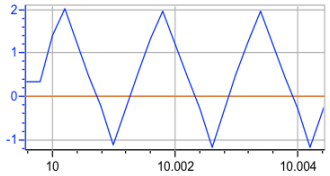
[0-1.5V]	10	184.63	0.0186	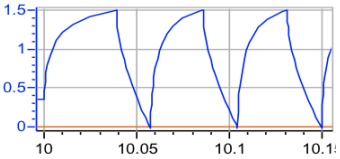
	50	24.70	0.0014	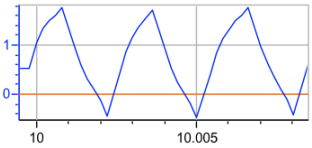
	100	19.99	<0.001 (resolution limit)	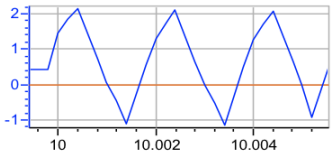
[0-2V]	10	3070 (51min10s)	0.1032	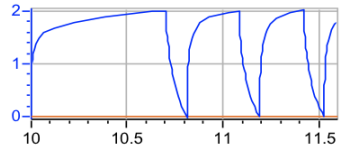
	50	61.00	0.0031	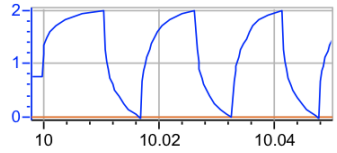
	100	21.90	<0.001 (resolution limit)	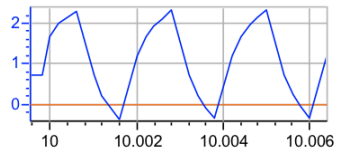

Chapter 6

Future work and perspectives

This final chapter explores different leads and perspectives for future research.

6.1 Energy generation: solar cells

The initial goal of the project was be to build a solar cell using vertically-aligned carbon nanotubes, based on a dye-sensitized solar cell platform.

The basic idea was to coat the vertically aligned carbon nanotubes with a layer of semiconductor titanium dioxide (TiO_2), whose role is to absorb the photon energy coming from the sunlight. Upon light excitation, the dye produces excitons that dissociates at the semiconductor-dye interface. The Coulomb force that maintains together the electron and the hole will be gone for a very short period of time such that the photo-excited electrons will then be transferred into the conduction band of the semiconductor and moved further towards the conducting plate (anode). On the other hand, the oxidized dye molecules are regenerated (reduced) by the electrolyte, which is commonly made of iodide/triodide redox couple.

The use of carbon nanotubes would have enhanced the transport of electrons and thus increased the quantity of energized electrons after illumination. This energy generation project was however soon abandoned when very encouraging results were found in the domain of energy storage.

6.2 Plastic behavior of nanotubes

This part was the most exciting and promising part, and was not explored due to time limitation. As previously stated, the specific capacitance was found to increase over time, in a very discreet way. After a couple of thousands cycles, a sudden jump in the specific capacitance was observed, where the value of the specific capacitance increases significantly by an order of magnitude.

Mechanical effects or deformation looks like the reason for this sudden increase. My hypothesis is that during charge and discharge, the CNT are deforming, an idea already proven in the case of SnO_2 nanowires by the article: *"In Situ Observation of the Electrochemical Lithiation of a Single SnO_2 Nanowire Electrode"*, (46). My guess is that some ions from the electrolyte are continuously penetrating the inner shell of the nanotubes, swelling them and increasing the diameter of the nanotubes until a critical point is reached, where the CNT enter a plastic deformation regime where it cannot be deformed anymore. The increase in volume induced by this plastic deformation, and thus of surface area available for reaction, explains such increase in specific capacitance. The hypothesis to be verified is that in the first thousands of cycles (this value differs from one experiment to another), the ions from the electrolyte fill the interior of the nanotubes until it is filled completely. The tube begins to swell gradually during the next thousands or tens of thousands of cycles, where the increase in volume of the nanotubes leads to the increase in specific capacitance observed in figure 6.1. A critical point is then reached when the nanotube cannot extend itself any more, and becomes brittle and distorted due to elongation in the vertical axis. It thus reached a plateau and either goes on working well for the next thousands of cycles as seen in figure 6.1, or breaks and fails, as seen in figure 6.2.

The way to check this hypothesis would be to run SEM, TEM and EDS before the experiment, then to run a charge-discharge experiment for hundreds of thousands of cycles. Once the experiment is stopped, the samples need to be dried with a critical point dryer to avoid the formation of bundles and then be seen again under SEM, TEM and EDS. A critical point drying is needed because when a liquid is introduced into the empty space between the nanotubes, the surface tension of the liquid starts to pull

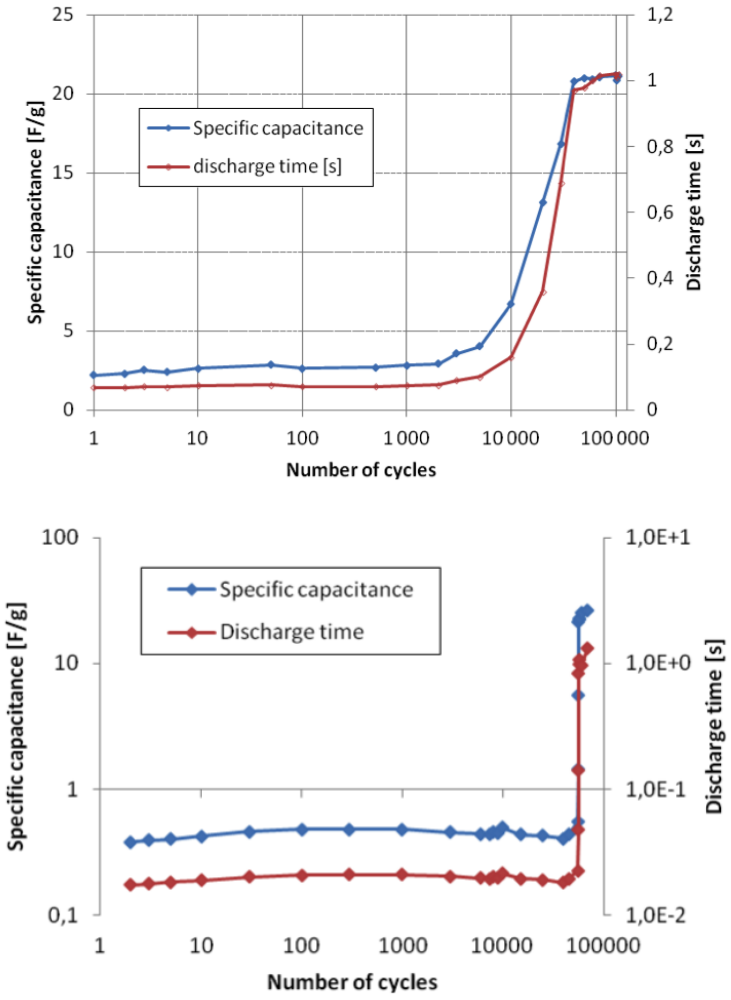

Figure 6.1: Plastic behavior of the nanotubes after thousands of cycles

the nanotubes closer such that the Van der Walls interactions is strong enough to agglomerate the VANT together, an effect known as 'zipping' (47). A critical point dryer avoid this effect by drying the nanotubes at the critical point temperature. Finally, a second round of SEM, TEM and EDS is needed to check if the nanotubes is indeed swelled, while the specific capacitance increased. Another (longer but more accurate) idea would be to examine the sample under SEM, TEM and EDS every ten thousand cycles to precisely correlate the increase of the diameter and length with the increase of specific capacitance.

However, this extremely exciting idea could not be completely pursued for different

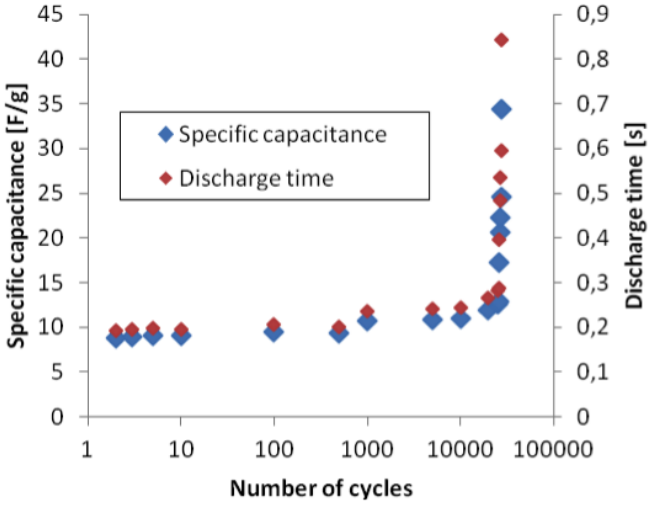

Figure 6.2: Destruction of the CNT array electrode - A second plateau can never be reached, the charge-discharge cycles break

reasons. First of all, the critical point dryer was part of another lab and it was difficult to have an access to it on such short notice due to an additional training. And second, this extremely time-consuming experiment would have required more than a month to conduct, which I did not have.

6.3 Fullerenes

Fullerenes are molecules made of 60 carbon atoms arranged in a series of interlocking pentagons and hexagons rings, forming a symmetrical spherical-shaped structure looking like a soccer ball, as depicted in figure 6.3. It is the roundest and most symmetrical large molecule known to man, and displays an astonishing array of amazing properties. With graphite and diamond, it is the third major form of pure carbon, and fosters some great promises in the field of energy storage.

In the same vein as the functionalization with -OH groups discussed previously, functionalization with fullerenes seemed to be an interesting and promising idea. The addition of fullerenes is expected to increase the overall surface area, and thus the storage capacity since it is proportional to the surface area of the electrodes. In addition to studying the effect of fullerenes themselves on as-grown nanotubes, it would have been

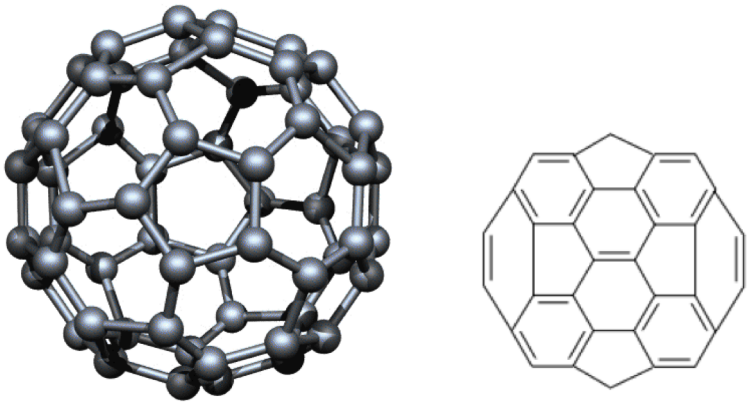

Figure 6.3: Representation of a Fullerene molecule

interesting to see the effect of functionalization with both -OH groups and fullerenes (hydrophilic nanotubes functionalized with fullerenes, $HiCNT_f$), and on hydrophobic nanotubes functionalized with fullerenes ($HoCNT_f$). $HiCNT_f$ are expected to give the best results, but different parameters are to be studied, thus it is still unsure if the addition of fullerenes groups can enhance or impede the action of -OH groups.

Lack of time for training in the deposition of fullerenes on the nanotubes resulted abandoning this interesting idea.

6.4 Gold particles

This subsection is drawn out from the idea presented in the article *"Nanoporous metal/oxide hybrid electrodes for electrochemical supercapacitors"* (44). This article demonstrates that hybrid structures made of nanoporous gold and nanocrystalline MnO_2 possesses enhanced conductivity, resulting in a specific capacitance of 1145 F/g, a value close to the theoretical value (a theoretical value of 1370 F/g is expected for a redox process involving one electron per manganese atom (48). The nanoporous gold allows electron transport through the MnO_2, and facilitates fast ion diffusion between the MnO_2 and the electrolytes while also acting as a double-layer capacitor.

Such tremendous values for specific capacitance are extremely appealing, and the idea of functionalizing carbon nanotubes with gold particles seems very promising. However, this encouraging design had to be left behind for similar reasons as before:

the training for depositing gold particles on the nanotubes was not possible in the remaining set time.

Chapter 7

Conclusion

This chapter provides a synthesis of the project and of its main results, and draws a general conclusion to the overall project.

7.1 Summary of the main results

Carbon nanotubes have been extensively demonstrated to be an extremely effective material for electrodes of energy storage devices due to their tremendous surface area, high electronic conductivity, lightweight and the interesting ability to be functionalized to optimize their capacitive properties. They are thus particularly well suited for use as supercapacitors, which can release a huge amount of stored energy within a very short period of time, thus making this device interesting for a vast range of applications.

The following results are worth being underlined:

- Through different electrolytes and multiple investigated parameters, carbon nanotube arrays were shown to be two to three times better than graphite in term of specific capacitance.

- The surface functionalization with hydroxyl groups was demonstrated to be a critical factor in both aqueous and non aqueous solutions to increase the specific capacitance.

- A maximum energy density of 21 Wh/kg at a power density of 1.1 kW/kg for a hydrophilic carbon nanotube electrode could be easily achieved using tetraethylammonium tetrafluoroborate in propylene carbonate. Respectively, a maximum power density was found to be 22 kW/kg at energy density of 2 Wh/kg for a hydrophobic carbon nanotube electrode.

These are encouraging results in the path of energy-storage devices with both high energy density and power density, using only carbon-based materials for the electrodes with a very long lifetime of more than hundreds of thousands of cycles.

7.2 Perspectives

Even though the performance obtained in this study is lower than what can be currently achieved using lithium-based electrolytes (average energy density of 45Wh/kg for supercapacitors (45), and specific capacitance of ∼135F/g for CNT-based electrodes (42), this carbon-based energy storage system still harvests a lot of advantages that skirt these lower values. First of all because the carbon nanotubes, as well as the copper and polypropylene filter, are inexpensive and are expected to be much cheaper in the near future. Moreover, the small ecological print of this device should be highlighted since most batteries use an electrolyte derived from lithium, which is not environmentally sound. According to the latest report of Meridian International Research, the mass production of lithium will cause great damage to endangered ecosystems (49). Moreover, lithium-based batteries will almost entirely be dedicated to portable electronics, not towards large-scale batteries for transportation or industrial use because the production can only sustain the portable electronics market (49). Thus, other materials for such large-scale batteries are yet to be found. This carbon-based energy storage system is also much less dangerous, since it does not carry the set of reactivity issues involved with lithium. The danger of a leak, leading to an explosion is not an issue with lithium-free carbon based EDLC.

Finally, the potential range chosen does not allow tremendous energy and power densities, but it does allow a lifetime of potentially more than hundreds of thousands of cycles. In comparison, most articles report a potential range from 0 to 3V (45), but the lifetime is only a few hundreds of cycles.

References

[1] International Energy Agency Statistics. **CO2 Emissions from Fuel Combustion: Highlights**. Technical report, International Energy Agency, 2010. 1

[2] World Energy Outlook (WEO 2009). **Reference Scenario**. Technical report, WEO, 2009. 1

[3] Intergovernmental Panel on Climate Change. **Fourth Assessment Report**. Technical report, IPCC, 2007. 1

[4] V.V.N. Obreja. **On the performance of commercial supercapacitors as storage devices for renewable electrical energy sources**. *Proceedings of International Conference on Renewable Energies and Power Quality (ICREPQ07)*, 2007. 2, 8

[5] P. Simon and Y. Gogotsi. **Materials for electrochemical capacitors**. *Nat. Mat*, **7**:845–854, 2008. 2

[6] Riccardo Signorelli and John G. Kassakian. **Electrochemical Double-Layer Capacitors Using Carbon Nanotube Electrode Structures**. *Proceedings of the IEEE*, **97**(11), 2009. 2, 5

[7] Elzbieta Frackowiak and François Béguin. **Carbon materials for the electrochemical storage of energy in capacitors**. *Carbon*, **39**:937–950, 2001. 3, 24

[8] Ray H. Baughman, Anvar A. Zakhidov, and Walt A. de Heer. **Carbon Nanotubes–the Route Toward Applications**. *Science 2*, **297**(5582):787–792, 2002. 3

[9] P.H.L. Notten, F. Roozeboom, R.A.H. Niessen, and L. Baggetto. **3-D Integrated All-Solid-State Rechargeable Batteries**. *Advanced Materials*, **19**(24):4564–4567, December 2007. 5

[10] GAMRY. *Testing Super-Capacitors Part 1 – CV, EIS and Leakage Current*. GAMRY Instruments. 6, 17

[11] Ch. Emmenegger, Ph. Maurona, P. Sudan, P. Wenger, V. Hermann, R. Gallay, and A. Züttel. **Investigation of electrochemical double-layer (ECDL) capacitors electrodes based on carbon nanotubes and activated carbon materials**. *Journal of Power Sources*, **124**(1):321–329, October 2003. 6

[12] Chenguang Liu, Zhenning Yu, David Neff, Aruna Zhamu, and Bor Z. Jang. **Graphene-Based Supercapacitor with an Ultrahigh Energy Density**. *Nano Letters*, **10**(12):4863–4868, 2010. 8, 9

[13] Jun Liu, Lixiang Yuan, Xiaoshuang Yang, Anthony Elbert, and Andrew T. Harris. **Synthesis of vertically aligned carbon nanotube arrays on polyhedral Fe/Al2O3 catalysts**. *Chem. Commun.*, pages 6434–6436, 2011. 12

[14] Elijah B Sansom, Derek Rinderknecht, and Morteza Gharib. **Controlled partial embedding of carbon nanotubes within flexible transparent layers**. *Nanotechnology*, **19**(3), 2008. 12

[15] Adrianus I. Aria and Morteza Gharib. **Reversible Tuning of Wettability of Carbon Nanotube Arrays: The Effect of UV/ozone and Vacuum Pyrolysis treatments**. *Langmuir*, 2011. 13, 14

[16] Peter T. Kissinger and William R. Heineman. **Cyclic Voltammetry**. *Journal of Chemical Education*, pages 702–706, 1983. 14, 15

[17] Francesco Lufrano and Pietro Staiti. **Conductivity and Capacitance Properties of a Supercapacitor Based on Nafion Electrolyte in a Nonaqueous System**. *Electrochemical and Solid-State Letters*, **7**(11):447–450, 2004. 15, 24

[18] Jingxing Chen, Nannan Xia, Tianxiang Zhou, Sanxiang Tan, Fengping Jiang, and Dingsheng Yuan. **Mesoporous Carbon Spheres: Synthesis, Characterization and Supercapacitance**. *International Journal of Electrochemical Science*, **4**:1063–1073, 2009. 15, 42

[19] Wei Chen, Zhongli Fan, Lin Gu, Xinhe Bao, and Chunlei Wang. **Enhanced capacitance of manganese oxide-via confinement inside carbon nanotubes**. *Chemical Communications*, **46**(22):3905–3907, 2010. 16

[20] Byoung-Yong Chang and Su-Moon Park. **Electrochemical Impedance Spectroscopy**. *Annual review of analytical chemistry Palo Alto California*, **3**(14):207–229, 2010. 17, 19

[21] GAMRY. *Basics of Electrochemical Impedance Spectroscopy*. GAMRY Instruments.

[22] Su-Moon Park, Jung-Suk Yoo, Byoung-Yong Chang, and Eun-Shil Ahn. **Novel instrumentation in electrochemical impedance spectroscopy and a full description of an electrochemical system**. *Pure Applied Chemistry*, **78**(5):1069–1080, 2006. 18

[23] Ludwig Reimer. *Scanning electron microscopy: physics of image formation and microanalysis*. Springer, 1998. 20

[24] Yang Leng. *Materials characterization: introduction to microscopic and spectroscopic methods*. Wiley, 2008. 21

[25] Anthony J. Garratt-Reed and David C. Bell. *Energy-dispersive X-ray analysis in the electron microscope*. BIOS Scientific Publishers, 2003. 21

[26] M. M. Shaijumon, F. S. Ou, L. Ci, and P. M. Ajayan. **Synthesis of hybrid nanowire arrays and their application as high power supercapacitor electrodes**. *Chem. Commun.*, pages 2373–2375, 2008. 21

[27] Victor L. Pushparaj, Manikoth M. Shaijumon, Ashavani Kumar, Saravanababu Murugesan, Lijie Ci, Robert Vajtai, Robert J. Linhardt, Omkaram Nalamasu, and Pulickel M. Ajayan. **Flexible energy storage devices based on nanocomposite paper**. *PNAS*, **104**(34):13574–13577, August 2007. 23, 24

REFERENCES

[28] A. G. Pandolfo and A. F. Hollenkamp. **Carbon properties and their role in supercapacitors**. *J. Power Sources*, **157**:11–27, 2006. 24

[29] Nanbu Noritoshi. **Thermal and electrolytic properties if quaternary ammonium salts based on fluorine-free chelatoborate anions and their applications to EDLCs**. *Electrochemical and Solid State Letters*, **9**(10):482–486, 2006. 25

[30] Richard Payne and Ignatius E. Theodorou. **Dielectric properties and relaxation in ethylene carbonate and propylene carbonate**. *J. Phys. Chem.*, **76**(20):2892–2900, 1972. 25

[31] Ralph P. Steward and Ernest C. Vieira. **The dielectric constants of ethylene carbonate and of solutions of ethylene carbonate in water, methanol, benzene and propylene carbonate**. -, 1967. 25

[32] S. Mitra, A. K.and Shukla, and S. Sampath. **Electrochemical capacitors based on sol-gel derived conducting composite solid electrolytes**. *Electrochem. Solid-State Lett*, **6**(8):149, 2003. 26

[33] S. A. Hashmi, R. J. Latham, R. G. Linford, and W. S. Schlindwein. **Studies on all solid state electric double layer capacitors using proton and lithium ion conducting polymer electrolytes**. *Journal of the Chemical Society, Faraday Transactions*, **93**(23), 1997. 26

[34] Tetsuya Osaka, Xingjiang Liu, Masashi Nojima, and Toshiyuki Momma. **An Electrochemical Double Layer Capacitor Using an Activated Carbon Electrode with Gel Electrolyte Binder**. *Journal of The Electrochemical Society*, **146**(5):1724–1729, 1999. 26

[35] Daniel T. Welna, Liangti Qu, Barney E. Taylor, Liming Dai, and Michael F. Durstock. **Vertically aligned carbon nanotube electrodes for lithium-ion batteries**. *Journal of Power Sources*, **196**:1455–1460, 2011. 26, 36, 42

[36] Chunsheng Du and Ning Pan. **Supercapacitors using carbon nanotubes films by electrophoretic deposition**. *Journal of Power Sources*, **160**:1487–1494, 2006. 27

[37] J. H. Chen, W. Z. Li, D. Z. Wang, S. X. Yang, J. G. Wen, and Z. F. Ren. **Electrochemical characterization of carbon nanotubes as electrode in electrochemical double-layer capacitors**. *Carbon*, **40**(8):1193–1197, 2002. 29

[38] Fujun Li, Madeleine Morris, and Kwong-Yu Chan. **Electrochemical capacitance and ionic transport in the mesoporous shell of a hierarchical porous core–shell carbon structure**. *J. Mater. Chem.*, **21**:8880–8886, 2011. 31

[39] Seung Woo Lee. **High power Li batteries from functionalized CNT electrodes**. *Nature Nanotechnology*, **5**:531–537, 2010. 35

[40] Andreas Hirsch. **Functionalization of Single-Walled Carbon Nanotubes**. *Angewandte Chemie International Edition*, **41**(11), 2002. 35

[41] Takayuki Iwasaki. **Highly selective growth of vertically aligned double-walled carbon nanotubes by a controlled heating method and their electric double-layer capacitor properties**. *Physica status Solidi (RRL)*, **2**(2):53–55, 2008. 38

[42] E. Frackowiak, K. Metenier, V. Bertagna, and F. Béguin. **Supercapacitor electrodes from multiwalled carbon nanotubes**. *Applied Physics Letters*, **77**(15), 2000. 38, 56

[43] Sherman. **Patent Sherman**. Patent, 2000. B.C.: US20006159933. 43

[44] Xingyou Lang, Akihiko Hirata, Takeshi Fujita, and Mingwei Chen. **Nanoporous metal/oxide hybrid electrodes for electrochemical supercapacitors**. *Nature Nanotechnology*, **6**:232–236, 2011. 44, 53

[45] L. Hu, J. W. Cho, Y. Yang, S. Jeong, F. La Mantia, L. Cui, and Y. Cui. **Highly conductive paper for energy-storage devices**. *PNAS*, **106**(51):21490–21494, 2009. 45, 56

[46] Jian Yu Huang, Li Zhong, Chong Min Wang, John P. Sullivan, Wu Xu, Li Qiang Zhang, Scott X. Mao, Nicholas S. Hudak, Xiao Hua Liu, Arunkumar Subramanian, Hongyou Fan, Liang Qi, Akihiro Kushima, and Ju Li. **In Situ Observation of the Electrochemical Lithiation of a Single SnO2 Nanowire Electrode**. *Science*, **330**(6010):1515–1520, 2010. 50

[47] Don N Futaba, Kenji Hata, Takeo Yamada, Tatsuki Hiraoka, Yuhei Hayamizu, Yozo Kakudate, Osamu Tanaike, Hiroaki Hatori, Motoo Yumura, and Sumio Iijima. **Shape-engineerable and highly densely packed single-walled carbon nanotubes and their application as super-capacitor electrodes**. *Nature Materials*, **5**(12):987–994, 2006. 51

[48] M. Toupin, T. Brousse, and D. Belanger. **Charge storage mechanism of MnO2 electrode used in aqueous electrochemical capacitor**. *Chem. Mater.*, **16**(3184–3190), 2004. 53

[49] Meridian International Research. **Report: The trouble with lithium 2: Under the microscope**. Technical report, Meridian International Research, June 2008. 56